# Models for Laser Ablation of Polymers

N. Bityurin,*[,†,‡] B. S. Luk'yanchuk,[‡] M. H. Hong,[‡] and T. C. Chong[‡]

*Institute of Applied Physics Russian Academy of Sciences, 603950, Nizhnii Novgorod, Russia, and Data Storage Institute, Agency for Science, Technology and Research, 117608, Singapore*

*Received May 31, 2002*

## Contents



*However, there is some difficulty in rightly determining the objects which we distinctly conceive.*

Rene Descarte

*The name "laser ablation" is used generally to describe the explosive laser-material interaction, a more appropriate definition that does not imply a mechanism.*

Site of the Lawrence Berkeley National Laboratory

*Thus, the definition of thinking is the creation and manipulation of symbols.*

Richard F. Taflinger

* Corresponding author, e-mail: bit@appl.sci-nnov.ru.
† Institute of Applied Physics Russian Academy of Sciences.
‡ Data Storage Institute.

## I. Introduction

UV laser ablation of polymers was discovered 20 years ago.[1,2] This effect has many fascinating applications in lithography, micromechanics, and medicine. For the last 20 years, more than $10^3$ papers describing this phenomenon were published (see, e.g., comprehensive reviews, refs 3−7). Despite the high research activity, the nature of UV laser ablation of polymers is still far from being fully understood, e.g., one can find contradictory interpretations of the same results in different papers.

Originally, UV laser ablation of polymers was believed to be a pure photochemical effect, resulting from the direct bond breaking by UV photons.[8−10] Gradually, investigators obtained evidence that laser heating of materials is significant and a pure thermal nature of laser ablation was considered.[11−13] Here we use the term "photothermal"[7] for the process resulting from laser heating of material.

Polymers are complex materials; therefore, laser ablation of polymers is also a complicated phenomenon. In this paper, we will focus on the models of laser ablation. In addition, we inevitably have to answer the question of what are the specific features of laser ablation of polymers that distinguish them from the laser ablation of other materials (metals, semiconductors, inorganic dielectrics, molecular solids).

There are several approaches to modeling of polymer ablation. The authors of this paper represent one of the "schools"; thus, our view of the problem is somewhat subjective.

Despite the complex nature of laser ablation, we prefer to develop simplified models (e.g., "pure" photochemical or "pure" photothermal), and analyze them in detail to be able to assign specific features, which are experimentally observed for a particular ablation mechanism.

We start with the photochemical model. In fact, the first consideration of laser ablation[10] employed a very simple but constructive idea that takes into account the specific feature of polymer materials. This idea is that polymers consist of long molecular chains with strong, covalent, bonds inside. At the same time, molecules belonging to different chains interact weakly. Therefore, polymer material becomes simple molecular solid (i.e., easily removed material), if we break the long polymer chains into small pieces by direct photochemical effect (UV photons are considered to have energy $\hbar\omega$ exceeding the energy of

10.1021/cr010426b CCC: $44.00 
Published on Web 01/28/2003

Nikita Bityurin was born in Nizhny Novgorod (Gorky), Russia, in 1954. He graduated from Nizniy Novgorod State University in 1977, and received his Ph.D. from Institute of Applied Physics Russian Academy of Sciences (IAP RAS). He has been with IAP RAS since 1977. During 1993–2002, he worked also as an Invited Researcher at Johannes Kepler University, Linz, Austria, LPL and LIMHP CNRS Laboratories, Villetaneuse, France, Data Storage Institute, Singapore, and as an Invited Professor at University Paris-Nord, France. His scientific interest is laser–matter interaction including laser effects on polymers, biological tissues and sol–gel materials. He published more than 70 papers in referred journals. At the moment, he is in the temporary position of the Head of Laboratory for Laser Processing of Materials at IAP RAS.

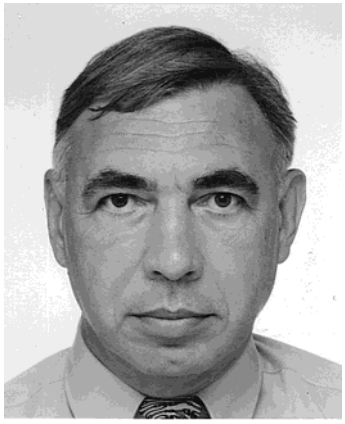

Boris Luk'yanchuk was born in Volgograd, Russia, in 1944. He graduated from the Moscow State University in 1967, and received his Ph.D. (1979) from the P. N. Lebedev Physical Institute, Russian Academy of Sciences and Doctor of Sciences (1991) from the General Physics Institute, Russian Academy of Sciences, and Professor's degree since 1992. During 1980–2000 was working as senior researcher and Head of the Laboratory at the General Physics Institute, Russian Academy of Sciences. Since 2000, he is working as member of technical staff of Data Storage Institute, Singapore. During 1989–2000, he was working as invited Professor in Johannes Kepler University, Linz, Austria, where he was awarded the title of Honorary Professor (1991). He was invited Professor at Faculté des Sciences de Luminy (Marseille, France), at Lecce University (Italy), and Tokyo Institute of Technology (Japan). He has published five monographs and more than 200 papers related to laser-matter interactions.

covalent bond). Taking into account the Bouguer–Lambert–Beer intensity distribution inside the material, this simplified consideration yields the so-called "photochemical law":[7]

$$h_e = \begin{cases} 0, & \text{if } \Phi < \Phi_{th} \\ \frac{1}{\alpha}\log\left[\frac{\Phi}{\Phi_{th}}\right] & \text{if } \Phi \geq \Phi_{th} \end{cases} \quad (1)$$

Here $h_e$ is the etch depth (per pulse), which is considered as a thickness of material, ablated per laser pulse, $\alpha$ is the absorption coefficient, $\Phi$ is the laser fluence, and $\Phi_{th}$ is the threshold fluence. This threshold fluence provides at the surface the fragments of polymer chains smaller than some characteristic length.[7] Typical value of this threshold fluence for polyimide and UV radiation with $\lambda = 193$ nm is about 15 mJ/cm$^2$.

Many authors used the dependence $h_e = h_e(\Phi)$ (we will call it kinetic curve) given by eq 1 to describe their experimental results. Later it was found that the value of $\alpha$ obtained by fitting the kinetic curve to experimental data could significantly differ from the measured absorption coefficient. It leads to the

Hong Minghui was born in Fujian, China, in 1965. He received his B.S. and M.S. from Physics Department, Xiamen University, in 1985 and 1988. After teaching in Xiamen University as an Assistant Professor from 1988 to 1994, he continued his M.E. (1996) and Ph.D. (2000) study in National University of Singapore. He joined Laser Microprocessing Group, Data Storage Institute, Singapore, in 1995 as a research engineer. Currently, he is the principal research engineer and deputy manager of the group. His research interest includes laser ablation and related applications.

Chong Tow Chong obtained his B.Eng. degree from the Tokyo Institute of Technology, his M.Eng. degree from the National University of Singapore, and his Sc.D. degree from the Massachusetts Institute of Technology, all in Electrical Engineering. He is currently the Director of the Data Storage Institute under the Agency for Science, Technology & Research and hosted by the National University of Singapore. Dr Chong's research interest is in the field of magnetic and optical data storage, especially in advance thin films for ultrahigh-density recording. He is also a Professor with the Department of Electrical and Computer Engineering, NUS. His other research interests include high-speed electronic and optical devices. Dr. Chong has authored and coauthored more than 120 publications in international refereed journals, presented 20 invited talks, and holds 16 patents. He serves as co-chairman of APMRC2002 and as member of the Technical Program Committee for ODS (USA), ISOM (Japan), MORIS (Japan), CLEO Pacific (USA), and OECC (Japan).

**Table 1. Calculated from Thermal Model and Experimental Values[13] of the Threshold Fluence**

| radiation $\lambda$, nm | $\alpha$, $10^5$ cm$^{-1}$ | $R$ | $\Phi_{th}$, mJ/cm$^2$, theory | $\Phi_{th}$, mJ/cm$^2$, experiment[13] |
|---|---|---|---|---|
| 351 | 0.32 | 0.1 | 102 | 105 |
| 308 | 1 | 0.11 | 46 | 46 |
| 248 | 3.1 | 0.12 | 29 | 25 |
| 193 | 4.25 | 0.07 | 26 | 15 |

idea of modification of optical properties of material during the pulse. This modification can be either nonreversible (leading to "incubation") or transient.[14,15]

In some papers, the kinetic curve is calculated based on the following consideration. The etch depth at a given fluence is considered as the distance from the surface at which the amount of absorbed energy per unit of volume equals the threshold one. The latter can be found from the data on ablation threshold. Usually it is implied that this absorbed energy provides a photochemical chain breaking; thus, these models can be treated in a similar way as photochemical.[15−19]

Photothermal modeling is another way to describe polymer ablation. It was understood that the absorbed energy produces an elevated temperature high enough for thermal destruction of the polymer. In ref 20, the etch depth is calculated as a penetration of isotherm where the temperature reaches its "critical" value, $T = T_{cr}$. Neglecting the heat diffusion one can write the adiabatic approximation for the increase in temperature:

$$\frac{dT}{dt} = \frac{\alpha I}{c_p \rho} \tag{2}$$

Here $I$ is the light intensity at a particular point, $c_p$ is the heat capacity, and $\rho$ is the density. Using the Bouguer-Lambert−Beer intensity distribution, one arrives at the "photochemical law" (eq 1) for the etch depth, where the threshold intensity is given by

$$\Phi_{th} = \frac{c_p \rho T_{cr}}{\alpha(1 - R)} \tag{3}$$

where $R$ is the reflection coefficient.

From a mathematical point of view, there is no difference between the above-formulated photochemical and photothermal models, i.e., the temperature plays the role of a "photochemical" variable. The both considerations yield the law (eq 1). Differences appear if one takes into account the heat diffusion.[20] A crude estimation can be done by replacing $\alpha^{-1} \rightarrow \alpha^{-1} + 2\sqrt{D_T t_p}$ in eq 3. Here $D_T$ is the heat diffusivity of polymer, and $t_p$ is the duration of a laser pulse. For illustration, we present in Table 1 the calculated values of the threshold fluence for laser ablation of polyimide by radiation of excimer lasers. The following values of parameters are used: $\rho = 1.4$ g/cm$^3$, $c_p = 2.2$ J/g K, $D_T = 10^{-3}$ cm$^2$/s, $T_{cr} = 850$ K, $t_p = 15$ ns. Experimental values of $\alpha$, $R$, and $\Phi_{th}$ are also presented in Table 1. One can see a very close correspondence of calculated and experimental results. In refs 21−23, the ablation is considered as a thermal destruction of polymer resulting from laser heating. Here heat diffusion is taken into account, and, most importantly, the ablation is associated with the chain breaking process, which obeys the Arrhenius law.

The introduction of the moving interface was a breakthrough from the point of view of modeling. Now it has been proved experimentally[24] that the interface between gaseous products of ablation and condensed material moves during the nanosecond laser pulse.

Historically, the problem with the moving interface was first considered in connection with the kinetics of the first-order phase transitions (movement of the melting front; see ref 7). Another problem with the moving interface was applied for the laser evaporation of metals.[25] There were several early attempts to construct models with a moving interface relating the problem of laser ablation of polymers.[26−31] These models are photochemical (even the model developed in ref 29 where the position of the front is associated with the critical temperature, but the temperature is calculated by eq 2).

Real thermal models with a moving interface following the model of ref 25 were developed for laser ablation of polymers in refs 32−36. We call them the "surface photothermal models" because they assumed photothermal destruction of the material within a very thin surface layer. It is similar to evaporation of heated material into vacuum. The velocity $V$ of ablation front follows the Arrhenius-like law:

$$V = V_0 \exp[-E_a/k_B T_s] \tag{4}$$

Here $V_0$ is of the order of sound velocity in condensed phase, $E_a$ is the activation energy of evaporation, $k_B$ is the Boltzmann constant, and $T_s$ is the surface temperature.

The consideration of moving interface problems immediately yields that the kinetic curve (near and above the threshold) should be linear rather than logarithmic. The logarithmic law (eq 1) at relatively high fluences is caused by attenuation of coming laser radiation within the plume. Thus, $\alpha$ in eq 1 is rather $\alpha_p$, a plume absorption coefficient recalculated per ablated depth, or Lagrange absorption coefficient of the plume. The absorbed laser intensity at the ablated surface is given by

$$I_s(t) = (1 - R) I_0(t) \exp[-\alpha_p h_e(t)] \tag{5}$$

where $I_0$ is incident laser intensity.

All the models considered in this paper are the models with a moving interface. We consider two types of such models, the so-called "Stefan-like" and "Frenkel-Wilson-like" problems.

With Stefan-like problems, the position of a moving interface is related to some critical value of the main variable. For example, in the classical Stefan problem of the melting front propagation it is melting temperature. In the theory of laser ablation of polymers, it would be rather the critical fracture of broken bonds. The position of interface within the Stefan-like problem is given in implicit form, similar to the position of the melt front, i.e., $T(z = z_{melt.front}) = T_{melt}$.

In the Frenkel-Wilson-like formulation, the velocity of a moving interface is a known function of values of variables at the surface. For example, for the melting problem one can write at some approximation (see in ref 7)

$$V_{\text{melt.front}} = \frac{dz_{\text{melt.front}}}{dt} \propto [T(z = z_{\text{melt.front}}) - T_{\text{melt}}]$$

Thus, overheating is a necessary condition for motion of the melt front, i.e., melting occurs only with $T(z = z_{\text{melt.front}}) > T_{\text{melt}}$. The classical surface photothermal model (eq 2) is also of the Frenkel-Wilson type because here the ablation velocity is a known function of surface temperature.

The paper is organized as follows. In section II, we consider the macrokinetic aspect of photochemical modification of polymers from a mathematical point of view. The photochemical modification of polymers under UV laser irradiation is their inherent feature (chain breaking is also a modification). Following refs 37−40, we formulate both Frenkel-Wilson and Stefan-like approaches to pure photochemical ablation. The main problem with the pure photochemical models is their self-consistency in the sense that we have to calculate the temperature rise which accompanies photochemical ablation. If the temperature is high enough to provide thermodestruction of the material, then the pure photochemical model is not reliable. This question is also discussed in section II.

In section III, we consider pure photothermal models of laser ablation. We start with the well-understood surface photothermal model.[35,36] Then we consider the Stefan-like and Frenkel-Wilson formulation of the so-called bulk or volume model where laser ablation proceeds through the chain scission caused by laser heating of material followed by surface evaporation of degradation products.[41−44] We compare the predictions of these models concerning ablation by nanosecond pulses.

In section IV, we consider application of these models for ablation by subpicosecond pulses. We compare predictions of surface and bulk models. Also we discuss here a model that is somewhat intermediate between photothermal and photochemical ones. It is the so-called photophysical model,[45−47] which is based on the reasonable assumption that activation energy of thermal decomposition of polymer chains can be smaller in the electronically excited state than in the ground state.

In section V, we consider other "intermediate models" (i.e., models between pure photochemical and pure photothermal). The necessity to develop these models is based, in particular, on recent experimental findings of influence of elevated temperatures on photochemistry.[48−49]

Section VI is devoted to the role of mechanical stresses in laser ablation. In fact, the importance of mechanical stresses for laser ablation has been discussed from the beginning of ablation era.[50] Mechanical stresses are caused either by thermoelasticity or by chemical changes during polymer modification.[50−59] As an example, one can refer to an increase in the volume of destruction products during the depolymerization of poly (methyl methacrylate) (PMMA). Another reason is the creation of volatile species, which produce inner pressure. There are models of laser ablation that relate the effect of ablation to some critical value of inner pressure.[60] In fact, these models come to the theory of polymer ablation from the theory of IR laser ablation of soft biological tissues. Here laser heating results in inner evaporation of water providing high-pressure inside the tissue. We consider in section VI how mechanical stresses can be incorporated in the models developed in the previous sections.

In the present paper, we do not address hydrodynamic and gas-dynamic aspects of laser ablation. Gas-dynamics of ablation is discussed in the recent review paper ref 61 and in refs 62−64.

We also do not consider melting[65] and topology of crater formation during ablation[66] as well as a very important question of stability of plain ablation front[67] and structure formation.[68−71] We believe that these problems will be discussed in a future review paper.

## II. Photochemical Ablation

### A. Photochemical Modification

Let us consider a laser beam propagating along the $z$ axis, the half-space $z > 0$ being occupied by the initially homogeneous dielectric media. We will evaluate equations that describe the photochemical modification of material in quite a general form. But first we consider the simplest photochemical reaction

$$\text{A} \xrightarrow{\hbar\omega} \text{B} \tag{6}$$

Here A stands for the element of the initial material, and B denotes the product of photochemical reaction. The kinetics of modification caused by eq 6 is described by the equations:

$$\frac{\partial N_{\text{A}}}{\partial t} = -\frac{\eta_{\text{A}}\sigma_{\text{A}}}{\hbar\omega} N_{\text{A}} I$$
$$\frac{\partial I}{\partial z} = -\alpha I \tag{7}$$
$$\alpha = \sigma_{\text{A}} N_{\text{A}} + \sigma_{\text{B}} N_{\text{B}}$$
$$N_{\text{A}} + N_{\text{B}} = N_0$$

Here $N_{\text{A}}$ and $N_{\text{B}}$ are the number densities of A and B species, respectively, $I$ is the light intensity, which is measured in W/cm$^2$, $\eta_{\text{A}}$ is the quantum yield, $\sigma_{\text{A}}$ and $\sigma_{\text{B}}$ are the absorption cross-sections, and $\alpha$ is the absorption coefficient. This model describes irreversibly induced darkening (for $\sigma_{\text{B}} > \sigma_{\text{A}}$) or bleaching (for $\sigma_{\text{B}} < \sigma_{\text{A}}$). We do not need a differential equation for $N_{\text{B}}$ since the conservation law $N_0 = \text{const}$.

The initial and boundary conditions are

$$N_{\text{A}}(z, 0) = N_0, \quad N_{\text{B}}(z, 0) = 0, \quad I(0, t) = I_s(t) \tag{8}$$

Here $I_s(t)$ can be an arbitrary function of time.

One can consider instead of eq 6 a more general model, which consists of two successive photochemical reactions:

$$A \xrightarrow{hv} B \xrightarrow{hv} C$$

In contrast to eq 6, this model can describe a no monotonous change of the absorption coefficient.

$$\frac{\partial N_A}{\partial t} = -\frac{\eta_A \sigma_A}{\hbar\omega} N_A I$$

$$\frac{\partial N_B}{\partial t} = \frac{\eta_A \sigma_A}{\hbar\omega} N_A I - \frac{\eta_B \sigma_B}{\hbar\omega} N_B I$$

$$\frac{\partial I}{\partial z} = -\alpha I \qquad (10)$$

$$\alpha = \sigma_A N_A + \sigma_B N_B + \sigma_C N_C$$

$$N_A + N_B + N_C = N_0$$

The initial and boundary conditions will be of the form (eq 8) with the additional condition $N_C(z,0) = 0$.

By a similar way, three, four, etc., successive or branching reactions can be taken into account to describe modification of material. If each step is caused by the photon absorption, then the kinetic equations will be of the form:

$$\frac{\partial S_m}{\partial t} = \Psi_m(S_1, S_2, ..., S_k) I, \quad m = 1, ..., k \qquad (11)$$

$$\frac{\partial I}{\partial z} = -\alpha(S_1, S_2, ..., S_k) I \qquad (12)$$

Here we introduce the set of $k$ variables $\{S_1, S_2, ..., S_k\}$. In the aforementioned models, this set consists of number densities $N_A$, $N_B$, and $N_C$. The boundary condition for intensity is similar to eq 8, i.e., $I(0,t) = I_s(t)$, and the initial conditions are

$$S_m(z,0) = S_{m,0} = \text{const}, \quad m = 1, ..., k \qquad (13)$$

This type of model was used in refs 16−19 as well in ref 72 when analyzing transient absorption during laser pulse and permanent modification of polymers by UV lasers. This kind of problem was considered in the 60s and in the 70s in physics of lasers, physics of plasma, and photochemical kinetics. The quite general form of photochemical kinetics was considered in refs 73 and 74. Comprehensive review can be found in ref 75 where such a kind of model was applied to investigate the photoaging of poly(vinyl chloride) (PVC).

By choosing an appropriate variable from the set $\{S_1, S_2, ..., S_k\}$ (let us denote it by $S$ and assume that $S = S_1$), we can reduce the set of $k$ eqs 11 to

$$\frac{dS_m}{dS} = \Psi_m(S_1, S_2, ..., S_k)/\Psi_1(S_1, S_2, ..., S_k), \quad m = 2, ..., k \qquad (14)$$

These $k$-1 ordinary equations with conditions $S_m(S_{1,0}) = S_{m,0}$ provide the expressions for $S_m$ as a function of $S$. Thus, we can introduce

$$S_m = S_m(S)$$

$$\Psi(S) \equiv \Psi_1(S, S_2(S), ..., S_k(S))$$

$$\alpha(S) \equiv \alpha(S, S_2(S), ..., S_k(S)) \qquad (15)$$

Hence, the set of eqs 11 and 12 can be reduced to a set of two equations:

$$\frac{\partial S}{\partial t} = \Psi(S) I, \quad \frac{\partial I}{\partial z} = -\alpha(S) I \qquad (16)$$

In what follows, we will discuss the set (eq 16) with the initial and boundary conditions:

$$S(z,0) = S_0 = \text{const} \qquad (17)$$

$$I(0,t) = I_s(t) \qquad (18)$$

The boundary condition for intensity is similar to eq 8. The general problem (eqs 16−18) can be solved analytically. From the first eq 16, we can express $I = \partial S/\partial t/\Psi(S)$. Then, the second eq 16 yields:

$$\frac{\partial}{\partial z}\left[\frac{\partial S}{\partial t}\middle/\Psi(S)\right] = -\alpha(S)\frac{\partial S}{\partial t}/\Psi(S)$$

It results in

$$\frac{\partial}{\partial t}\left[\frac{\partial S}{\partial z}\middle/\Psi(S) + \int_{S_0}^{S} \frac{\alpha(S')}{\Psi(S')} dS'\right] = 0 \qquad (19)$$

Taking into consideration the initial conditions (eq 17) provides:

$$\frac{\partial S}{\partial z} = -\Psi(S) \int_{S_0}^{S} \frac{\alpha(S')}{\Psi(S')} dS' \qquad (20)$$

Integrating ordinary differential eq 20 yields the solution that we present in the form, which is convenient for the future:

$$z - z_0 = \int_{S(z)}^{S(z_0)} \frac{dS''}{\Psi(S'') \int_{S_0}^{S''} \frac{\alpha(S')}{\Psi(S')} dS'} \qquad (21)$$

Here $z_0$ is some fixed coordinate inside the material ($z_0 \geq 0$). In particular, taking $z_0 = 0$ provides:

$$z = \int_{S}^{S(0,t)} \frac{dS''}{\Psi(S'') \int_{S_0}^{S''} \frac{\alpha(S')}{\Psi(S')} dS'} \qquad (22)$$

The implicit expression for $S(0,t)$ can be obtained from the first eq 16 and the boundary conditions (eq 18):

$$\int_{S_0}^{S(0,t)} \frac{dS''}{\Psi(S'')} = \int_0^t I_s(t) dt \qquad (23)$$

There are several important properties of eqs 22 and 23. First, the distribution of $S_i$ ($i$ = 1,..., $k$) variables depends not on the time by itself but rather

on the integrated dose $\int_0^t I_s(t)dt$, see eq 23. It follows from eq 20 that spatial derivative of $S$ at each point within the sample depends only on $S$; that is, knowing $S$ at the particular point, we know the derivative $\partial S/\partial z$. Equation 22 can be expressed in the form:

$$z = f_1(S) + \Omega(t) \tag{24}$$

where

$$f_1(S) = \int_S^{S_{\text{fixed}}} \frac{dS''}{\Psi(S'')\int_{S_0}^{S''}\frac{\alpha(S')}{\Psi(S')}dS'}$$

and

$$\Omega(t) = \int_{S_{\text{fixed}}}^{S(0,t)} \frac{dS''}{\Psi(S'')\int_{S_0}^{S''}\frac{\alpha(S')}{\Psi(S')}dS'}$$

Here $S_{\text{fixed}}$ is an arbitrary fixed value of $S \neq S_0$. Equation 24 can be rewritten:

$$S(z,t) = P_S(z - \Omega(t)) \tag{25}$$

Here $P_S = f_1^{-1}$. Equation 25 means that the evolution of distribution of $S$ inside the material can be represented as propagation of a nondeformable profile (wave of modification) $P_S(\xi)$ with time-dependent velocity

$$V_{\text{mod}}(t) = \frac{d\Omega}{dt} = \frac{I_0(t)}{\int_{S_0}^{S(0,t)}\frac{\alpha(S)}{\Psi(S)}dS} \tag{26}$$

Henceforth this velocity will be referred to as the velocity of the wave of modification. The shape of this profile obeys eq 20 with $S(z) = P_S(z)$. Similarly, it can be shown directly that the solution for each $S_i$ variable can be represented as

$$S_i(z,t) = P_{S_i}(z - \Omega(t)) \tag{27}$$

where $P_{S_i}(\xi)$ is the corresponding profile, $P_{S_i}(\xi) = S_i(P_S(\xi))$.

These profiles have the property: $P_{S_i}(\infty) = S_{i,0}$. At $t = 0$ the profile is situated at $z = -\infty$. At $t = 0$, $V_{\text{mod}} = \infty$. The above symmetry of eqs 24 and 25 has been recognized for the first time in refs 75 and 76.

To finish the consideration of the macroscopic theory of photochemical modification, let us consider the special choice of the variable $S$. To avoid any confusion, let us denote it $\bar{S}$. Thus, we *add* to the set $\{S_i\}$ ($i = 1,..., k$) one more, $k + 1$ variable, $\bar{S}$, which obeys the equation of the type of eq 11:

$$\frac{\partial \bar{S}}{\partial t} = I; \quad \bar{S}(z,0) = 0 \tag{28}$$

According to eq 29

$$\bar{S}(z,t) = \int_0^t I(z,t)dt \tag{29}$$

is the integrated dose, which *come* to the point $z$ before the moment of time $t$.

We chose $S = \bar{S}$. Now we have $\Psi(\bar{S}) = 1$, and all the formulas become simpler. $S_m(\bar{S})$ can be found from the set of ordinary equations:

$$\frac{dS_m}{d\bar{S}} = \Psi_m(S_1,S_2,...,S_k), \quad m = 1,...k \tag{30}$$

$$\alpha(\bar{S}) = \alpha(S_1(\bar{S}),S_2(\bar{S}),...,S_k(\bar{S})) \tag{31}$$

$$\bar{S}_0 = 0 \tag{32}$$

$$\bar{S}(0,t) = \int_0^t I_s(t)dt \tag{33}$$

$$\frac{\partial \bar{S}}{\partial z} = -\int_0^{\bar{S}} \alpha(\bar{S}')d\bar{S}' \tag{34}$$

$$z = \int_{\bar{S}}^{\bar{S}(0,t)} \frac{d\bar{S}''}{\int_0^{\bar{S}''}\alpha(\bar{S}')d\bar{S}'} \tag{35}$$

## B. Single-Step Model

Let us apply the above formalism to the simplest single-step model (eqs 6−8), which can be considered as one of the basic models for laser induced photomodification. The set of equations here has the form eqs 16−18. As variable $S$ we can choose $N_A$, then $\Psi = -\eta_A\sigma_A/\hbar\omega\ N_A$ and $\alpha = \sigma_A N_A + \sigma_B(N_0 - N_A)$. To represent corresponding formulas in compact form, it is convenient to introduce dimensionless variables

$$n_A = \frac{N_A}{N_0}, \quad n_B = \frac{N_B}{N_0}, \quad \tau = \frac{\eta_A\sigma_A}{\hbar\omega}\int_0^t I_s(t_1)dt_1,$$
$$\xi = \sigma_A N_0 z \tag{36}$$

and dimensionless parameter $\beta = \sigma_B/\sigma_A$.

Dimensionless time $\tau$ is integrated dose normalized by characteristic dose $\hbar\omega/\eta_A\sigma_A$. The coordinate scale is an initial light penetration depth. The value of the parameter $\beta$ controls the type of irreversible optical modification (bleaching at $\beta < 1$ or darkening at $\beta > 1$).

In dimensionless variables the ordinary differential equation for the space distribution (eq 20) becomes:

$$\frac{dn_A}{d\xi} = (1 - \beta)(1 - n_A)n_A - \beta n_A \log(n_A) \tag{37}$$

The boundary value (see eq 23) reads:

$$n_A(\xi = 0,t) = \exp(-\tau) \tag{38}$$

The velocity of the wave of modification (eq 26) yields:

$$V_{\text{mod}} = \frac{1}{(1 - \beta)(1 - \exp(-\tau)) + \beta\tau} \tag{39}$$

Solution of the eqs 37 and 38 is shown in Figure 1. One can see the propagating wave of photochemical modification along the $\xi$ coordinate. As it is explained above, this solution describes some universal profile obeying eq 37 moving with respect to coordinate with the velocity (eq 39) in such a way that the boundary relation (eq 38) holds.

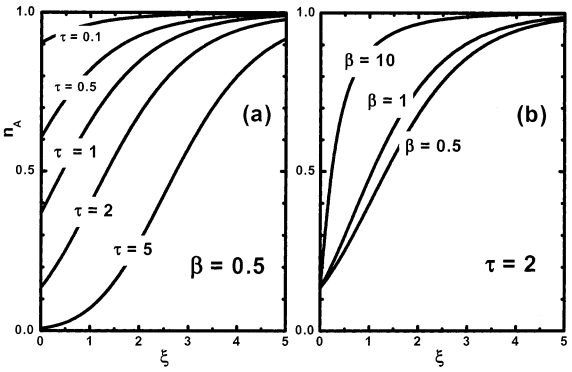


**Figure 1.** Wave of photochemical reaction; profiles $n_A = n_A(\xi)$ obtained from integration of eq 37 for fixed parameter $\beta = 0.5$ (a) and for fixed parameter $\tau = 2$ (b). With $\beta < 1$, one has the bleaching effect and with $\beta > 1$ the darkening effect.

The profile of $n_B$ variable can be obtained from the $n_A$ profile as

$$n_B = 1 - n_A \tag{40}$$

The profile for dose variable $\bar{S}$ (see eq 33), or rather for dimensionless $\bar{s} = \eta_A \sigma_A / \hbar\omega \; \bar{S}$, obeys the equation (see eq 34):

$$\frac{\partial \bar{s}}{\partial \xi} = (\beta - 1)(1 - \exp(-\bar{s})) - \beta \bar{s}$$

$$\bar{s}(\xi = 0, t) = \tau$$

For both $n_B$ and $\bar{s}$ profiles the velocity of propagation is the same as for $n_A$ (eq 39).

## C. Surface Photochemical Etching (The Frenkel-Wilson Approach)

In this section, we consider the problem of photochemical modification with a moving interface. We start with the Frenkel-Wilson approach to this problem. The results can be applied to analysis of photochemical etching when photomodified material is etched due to surface photochemical reaction with surroundings.

During etching, a part of the material is removed from the surface of the sample. As a result, the problem with the moving interface arises. There are two approaches to the formulation of this problem. The first one is similar to the Frenkel-Wilson approach in the theory of melting front propagation.[7] Within this approach, the ablation velocity is considered as a function of intensity and the values of variables $\{S_i\}$ at the moving interface. This approach for the photochemical theory of UV etching was developed in ref 37.

We consider the model with eqs 11 and 12 and moving interface positioned at $z = z_s(t)$. Instead of eq 18, we consider the boundary condition of the form:

$$I(z_s, t) = I_s(t) \tag{41}$$

Henceforth, we use the subscript $s$ for surface values of the variables.

With the Frenkel−Wilson approach we consider the etching velocity

$$\frac{dz_s}{dt} = V_{\text{etch}}(S_{1,s}, S_{2,s}, \ldots, S_{k,s}, I_s) \tag{42}$$

It is important that $V_{\text{etch}}(S_{1,s}, S_{2,s}, \ldots, S_{k,s}, I_s)$ is *a known function*. Thus, we can express $S_i$ through $S$ as in eq 15 with $S_s(t) \equiv S_{1,s}(t)$. Similar to eq 15, we can introduce the etching velocity in the form

$$\frac{dz_s}{dt} = V_{\text{etch}}(S_s(t), I_s(t)) \tag{43}$$

It is evident that, before the etching front reaches a particular point, for this point etching will manifest itself only by some changes in upcoming light intensity. It means that eq 20 works for all inner points and at the very surface as well.

At each moment of time relation holds:

$$\frac{dS_s(t)}{dt} = \left.\frac{\partial S(z,t)}{\partial z}\right|_{z=z_s} \cdot \frac{dz_s}{dt} + \left.\frac{\partial S(z,t)}{\partial t}\right|_{z=z_s} \tag{44}$$

The value of $\partial S(z,t)/\partial t|_{z=z_s}$ can be found from the first of eq 16:

$$\left.\frac{\partial S(z,t)}{\partial t}\right|_{z=z_s} = \Psi(S_s) I_s(t) \tag{45}$$

The value of $\partial S(z,t)/\partial z|_{z=z_s}$ can be found from eq 20:

$$\left.\frac{\partial S}{\partial z}\right|_{z=z_s} = -\Psi(S_s) \int_{S_0}^{S_s} \frac{\alpha(S')}{\Psi(S')} dS' \tag{46}$$

Thus, eqs 44−46 yield:

$$\frac{dS_s}{dt} = \Psi(S_s) I_s \left\{ 1 - \frac{V_{\text{etch}}(S_s, I_s)}{V_{\text{mod}}(S_s, I_s)} \right\}, \quad S_s(0) = S_0 \tag{47}$$

where $V_{\text{etch}}(S_s, I_s)$ is given by eq 43, and $V_{\text{mod}}(S_s, I_s)$ is given by eq 26:

$$V_{\text{mod}}(S_s, I_s) = -\frac{I_s}{\int_{S_s}^{S_0} \frac{\alpha(S')}{\Psi(S')} dS'} \tag{48}$$

From the above section, it is obvious that the considered process can be represented as the propagation of the wave of modification and the front of etching. The etching front propagates with the velocity (eq 43), while the modification wave propagates with the velocity (eq 48). Generally, $V_{\text{etch}} \neq V_{\text{mod}}$. It is important that $S_s(t)$ obeys a closed ordinary differential eq 47. Solving eq 47, one obtains $S_s(t)$. Substituting this function in eq 43, one yields the dependence $V_{\text{etch}} = dz_s/dt$.

The coordinate distribution of modification products in the remaining part of the sample at the moment $t$, $S(z,t)$ can be obtained from eq 21:

$$z - z_s = -\int_{S_s(t)}^{S} \frac{dS''}{\Psi(S'') \int_{S''}^{S_0} \frac{\alpha(S')}{\Psi(S')} dS'} \tag{49}$$

Thus, we reduced the set of partial differential eqs 11−13, 41, and 42 into a set of ordinary differential eqs 20 and 47. Equation 49 is another form of eq 20. Thus, the kinetics of photochemical surface etching can be represented as propagation of profiles $P_{S_i}(\xi)$ with the velocity (eq 48) accompanied by propagation of the etching front. Ordinary differential equation 47 allows one to obtain the surface value of each $\{S_i\}$ variable involved as a function of time. It allows one to build the spatial distribution of each variable at each moment of time using eq 20 or eq 49.

Let us consider a particular case when $I_s = \text{const}$. Here the condition $V_{\text{etch}} = \text{const}$ in time corresponds to a stationary wave solution and is equivalent to the condition $dS_s/dt = 0$, or $S_s = \text{const}$. This constant, let us designate it $S_s^*$, obeys the equation:

$$\Psi(S_s^*)I_s\left\{1 - \frac{V_{\text{etch}}(S_s^*,I_s)}{V_{\text{mod}}(S_s^*,I_s)}\right\} = 0$$

or, in physical cases:

$$V_{\text{etch}}(S_s^*,I_s) = V_{\text{mod}}(S_s^*,I_s) \tag{50}$$

It means that the stationary modification and etching waves propagate with the same velocity. As it is seen from eq 50, $S_s^*$ generally depends on intensity. Because $S_s = \text{const}$, the spatial distribution of all the $\{S_i\}$ variables will not change in time if we fix the reference frame with the moving interface. This stationary wave solution can serve as an attractor, i.e., the solution of the problem can tend to the stationary wave.

If etching velocity is proportional to intensity

$$V_{\text{etch}}(S_s,I_s) = \bar{V}_{\text{etch}}(S_s)I_s \tag{51}$$

then

$$\frac{V_{\text{etch}}(S_s,I_s)}{V_{\text{mod}}(S_s,I_s)} = \bar{V}_{\text{etch}}(S_s)\int_{S_0}^{S_s}\frac{\alpha(S')}{\Psi(S')}dS'$$

As a result, eq 47 becomes an equation with separating variables and can be solved in quadratures. Introducing a new time variable (surface dose):

$$\tau_s = \int_0^t I_s(t)dt$$

one can transfer eq 47 into the following form:

$$\frac{dS_s}{d\tau_s} = \Psi(S_s)\left(1 - \bar{V}_{\text{etch}}(S_s)\int_{S_0}^{S_s}\frac{\alpha(S')}{\Psi(S')}dS'\right); \quad S_s(0) = S_0 \tag{52}$$

The stationary value $S_s^*$ obeys the equation (see eq 50):

$$\tilde{V}_{\text{etch}}(S_s^*)\int_{S_0}^{S_s^*}\frac{\alpha(S')}{\Psi(S')}dS' = 1 \tag{53}$$

where $S_s^*$ does not depend on the intensity.

This stationary solution does not propagate with constant velocity with respect to real time if $I_s(t) \neq \text{const}$, etching velocity is proportional to intensity according to eq 51, but the spatial distributions of all the $\{S_i\}$ variables will not change in time if we fix the reference frame with the moving interface.

## D. Single Step Model. Results and Discussion

Let us apply general formalism to the particular case of model (eq 6). Along with the eqs 7, we introduce the expression for the surface etching velocity, assuming its linear dependence on $N_A$ and $N_B$. Thus

$$V_{\text{etch}} = (G_A N_A + G_B N_B)I_s \tag{54}$$

The problem (eqs 7 and 54 may be rewritten in dimensionless variables (eq 36)):

$$\frac{\partial n_A}{\partial \tau} = -n_A q; \quad \frac{\partial q}{\partial \xi} = -n_A q - \beta(1 - n_A)q;$$
$$\frac{d\xi_s}{d\tau} \equiv \tilde{V}_{\text{etch}} = \nu\{n_A(\xi_s) + g[1 - n_A(\xi_s)]\} \tag{55}$$
$$\xi_s(\tau = 0) = 0; \quad q(\xi_s) = 1; \quad n_A(\xi_s = 0) = 1$$

Here $\xi_s(\tau)$ is the dimensionless position of the etch front. $q = I/I_s$ is the dimensionless intensity, $q(\xi_s)$, $n_A(\xi_s)$ are the values of variables at the interface. The discussed problem is characterized by three dimensionless parameters involved: $\beta = \sigma_B/\sigma_A$; $g = G_B/G_A$; $\nu = G_A N_0^2/\eta_A$.

To use mathematical formalism developed in section IIC, we assign (see above):

$$n_A = S, \quad \Psi(S) = -S, \quad S_0 = 1$$

The dimensionless modification velocity, see (eq 48), and etching velocity as a function of surface value $S_s \equiv n_A(\xi_s)$ read:

$$V_{\text{mod}} = \frac{1}{(1 - S_s)(1 - \beta) - \beta \log S_s} \tag{56}$$

$$\tilde{V}_{\text{etch}} = \nu[S_s + g(1 - S_s)] \tag{57}$$

Thus, the main eq 47 or 52 becomes:

$$\frac{dS_s}{d\tau} = -S_s[\nu S_s + g(1 - S_s)][\beta \log S_s - (1 - S_s)(1 - \beta) + 1]; \quad S_s(0) = 1 \tag{58}$$

This is an ordinary differential equation allowing one to obtain the dependence $S_s(\tau)$. Substituting this solution into (eq 57), one finds the dependence $\tilde{V}_{\text{etch}}(\tau)$. Dose dependence of etch depth, $h_e$, can be found by integrating

$$h_e(\tau) = \frac{1}{\sigma_A N_0}\int_0^\tau \tilde{V}_{\text{etch}}(\tau)d\tau \tag{59}$$

In eq 59, $\sigma_A N_0$ is the initial absorption coefficient. Integrated dose (J/cm$^2$) is $\tau \times \hbar\omega/\sigma_A\eta_A$. When comparing with experimental data $\hbar\omega/\sigma_A\eta_A$ also serves as an important parameter.

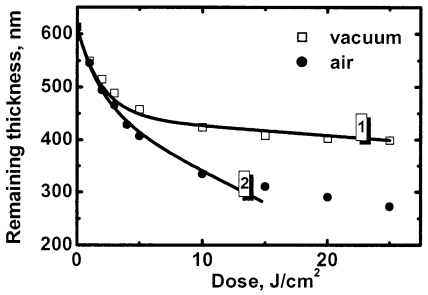


**Figure 2.** Fitting of experimental data on UV photochemical etching by surface etching model. Experimental data are from ref 77. Irradiation of PMMA films was performed by the fifth harmonic of Nd:YAP laser at $\lambda = 216$ nm. Circles − irradiation in air. Squares − irradiation in a vacuum ($5 \times 10^{-3}$ Torr). Solid curves correspond to the calculations according to the model discussed in section IID (eqs 57−59). For both curve 1 and 2, $\beta = 15$, $\hbar\omega/\eta_A\sigma_A = 1.754$ J/cm$^2$, $\nu = 0.05$. Curve 1 is calculated with $g = 0.02$. Curve 2 corresponds to $g = 0.13$. It is seen that fitting is good while the thickness of the film is large enough. (Reprinted with permission from ref 37. Copyright 1999 Elsevier Science.)

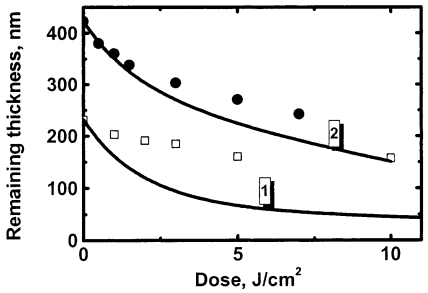


**Figure 3.** The same as in Figure 2, but the initial thickness of the film is different. It is seen that the considered model cannot fit the experimental data for relatively thin films. (Reprinted with permission from ref 37. Copyright 1999 Elsevier Science.)

We apply this model to fit the data on UV etching of PMMA films by the fifth harmonic of Nd:YAP laser[77] (see in Figure 2). This solid-state neodymium laser operates at the wavelength $\lambda = 1.08$ $\mu$m; thus, the wavelength of the fifth harmonic is $\lambda = 216$ nm. We use the values of parameters $\hbar\omega/\sigma_A\eta_A = 1.754$ J/cm$^2$, $\beta = 15$, and $\nu = 0.05$ both in air and in a vacuum. The difference between curves 1 and 2 in Figure 2 results from the difference in values of the coefficient $g$. Hence, the appropriate values for air environment and for a vacuum are $g = 0.13$ and $g = 0.02$, correspondingly. It means that the virgin material is etched irrespective of the environment, whereas the modified material is etched much more effectively in air than in a vacuum. It is quite natural bearing in mind that UV modification of PMMA leads to the creation of unsaturated carbon bonds. It is seen in Figure 3 that this model fails when film thickness is small enough. The present model cannot explain the dependence of the etch rate on the initial thickness of the film. Here bulk models[77,78] should be applied.

It is worth noting, nevertheless, that the fitting experimental data by the bulk model yields the same values for parameters $\beta$ and $\hbar\omega/\sigma_A\eta_A$. Thus, there is some correspondence between the two models describing the limiting cases.

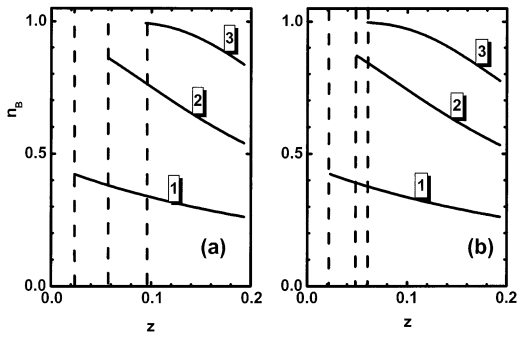


**Figure 4.** Spatial distributions of $n_B$ component, calculated from eqs 57−59, 37, and 40. Curves 1, 2, and 3 correspond to moments of time $\tau = 0.57$, 2.28, 6.84. Left (dotted) borders present the moving boundary. The initial film thickness was 6130 Å. Spatial coordinate in dimensionless units (value 0.2 corresponds to the film−substrate interface). (a) Values of parameters correspond to curve 2 in Figure 2, i.e., irradiation in air, parameter $g = 0.13$. (b) Values of parameters correspond to curve 1 in Figure 2, i.e., irradiation in a vacuum, parameter $g = 0.02$. (Reprinted with permission from ref 37. Copyright 1999 Elsevier Science.)

Figure 4 exhibits calculated kinetics of etching accompanied by modifications for irradiation in air and in a vacuum. The distributions of concentration $n_B$ in different moments of time and in different environments are parts of the same profile described by the eqs 37 and 40. In air, the etch rate is larger than in a vacuum. Nevertheless, in both cases, the modification velocity appears to be significantly larger than the etching velocity. Thus, the solutions are quite far from the stationary waves. It means that in the considered cases the process is essentially nonstationary.

## E. Photochemical Theory of Laser Ablation. The Stefan-like Approach

In this section, following refs 37−40, we consider another approach that can be called the Stefan-type approach because it is similar to Stefan's set of the problem of a moving melting front. Here the moving interface is fixed with the defined value of one of the $S_i$ variables. When considering the ablation of polymers, the appropriate variable is the number density of broken bonds. When number density of broken bonds at the surface reaches its critical value, ablation starts and hereafter the position of the interface will be fixed with this critical value of the broken bonds which corresponds to the critical value of the averaged length of polymer chains. Thus, this condition means that when polymer chains at the interface become short enough, they leave the surface. This consideration is quite natural and has been used since the first papers of Srinivasan et al. (see e.g., ref 10).

The development of suitable VUV laser sources with wavelength shorter than usually employed[79,80] excimer $F_2$ lasers[81] provides a new opportunity for laser treatment of materials with a great accuracy and a small lateral resolution. VUV ablation of polymers is one of the promising areas of application for newly developed laser technique.[82] The advent of VUV lasers with the photon energy as high as 10 eV

and their use for irradiation of polymers increases once again the interest to the theory of laser ablation, where the most intriguing point is the interrelation between thermal and nonthermal processes. From the very beginning of UV laser ablation modeling, it was believed that polymer ablation is dominated by direct photochemical main-chain scission.[10] The comprehensive investigations[83] have shown, however, that, at least for the so largely studied and used polymer as PMMA, only with VUV the direct photochemical main-chain scission can be really relevant to the laser ablation process.

The problem is how to include correctly the modifications and moving interface. It should be noted that the Stefan-type problem for polymer ablation, when chain scission is a solely thermally activated process, was comprehensively studied in ref 42 and will be discussed within the next sections.

Similar to section IIB, we consider the eqs 11 and 12 reduced to eqs 16 and 17 with a moving interface $z_s$ and with a boundary condition (eq 41). Now eq 42 is not valid and the time dependence of ablation velocity

$$V(t) = \frac{dz_s}{dt} \tag{60}$$

should be obtained from the Stefan-like condition:

$$S_s = S_{cr} = \text{const} \tag{61}$$

where the value $S_{cr}$ corresponds to critical value of the number density of broken bonds.

Now we once again consider eq 44:

$$\frac{dS_s(t)}{dt} = \left.\frac{\partial S(x,t)}{\partial x}\right|_{z=z_s} \cdot V(t) + \left.\frac{\partial S(x,t)}{\partial t}\right|_{z=z_s} \tag{62}$$

From eq 61, it follows that in our case $dS_s(t)/dt = 0$ and from eq 62 one obtains the expression for the ablation velocity:

$$V(t) = -\left.\frac{\partial S(x,t)}{\partial t}\right|_{z=z_s} \Big/ \left.\frac{\partial S(x,t)}{\partial x}\right|_{z=z_s} = I_s(t) \Big/ \int_{S_0}^{S_{cr}} \frac{\alpha(S')}{\Psi(S')} dS' \tag{63}$$

Equation 63 suggests that, when $S_{cr}$ is fixed, the ablation velocity is proportional to light intensity at the surface and its dependence on time entirely follows the time dependence of surface intensity. Thus, we can write:

$$V(t) = \frac{I_s(t)}{\hbar\omega\kappa_{ph}} \tag{64}$$

Here $\kappa_{ph}$ is a constant. To understand the physical meaning of this constant, let us make a special choice of the variable $S$ (see eq 28). Now we have $\Psi(\bar{S}) = 1$ and

$$\kappa_{ph} = \frac{1}{\hbar\omega} \int_0^{\bar{S}_{cr}} \alpha(\bar{S}) d\bar{S} \tag{65}$$

According to eq 29, $\bar{S}(z,t) = \int_0^t I(z,t)dt$ is the integrated dose, which *comes* to the point $z$ before the moment of time $t$. It means that $\kappa_{ph}$ *is the number density of photons, which should be absorbed at this particular point to produce critical number density of broken bonds at this point.*

Ablation velocity (eq 63) coincides exactly with the velocity of modification (eq 26). According to section II.D, it means that the spatial distributions of all the $\{S_i\}$ variables will not change in time if we fix the reference frame with the moving interface.

Let us consider now single-pulse and multipulse ablation kinetics within the photochemical ablation model.

Equation 63 has been written in the assumption that the number density of broken bonds at the surface corresponds to its critical value. Initially, however, we have no broken bonds at the surface of the material.

If pulse fluence is not enough to produce the critical number of broken bonds at the surface, then there would be no ablation at all. Thus, there is some threshold fluence $\Phi_{th}$, which can be estimated from the following considerations.

We introduce pulse fluence $\Phi = \int I_0 dt$ (for rectangular pulse $\Phi = \int_0^{t_p} I_0(t)dt$, where $t_p$ is laser pulse duration). Here $I_0(t)$ is the laser intensity. For an immovable interface the nonreflected intensity at the surface is given by

$$I_s(t) = I_0(t)[1 - R(\{S_i(t)\})] = I_0(t)[1 - R(\bar{S}(t))] \tag{66}$$

Here all the values of variables are taken at the surface.

Combining eqs 28 and 66 easily yields:

$$\Phi_{th} = \int_0^{\bar{S}_{cr}} \frac{d\bar{S}}{1 - R(\bar{S})} \tag{67}$$

If $\Phi > \Phi_{th}$ the interface will move according to the law (eq 64) during the time $t_{cr} < t \le t_p$ where $t_{cr}$ obeys the equation $\int_0^{t_{cr}} I_0(t)dt = \Phi_{th}$. Since the interface starts moving, the surface intensity $I_s(t)$ will be connected with $I_0(t)$ through the absorption within the plume. Assuming the simplest model of plume absorption we can write (for $t > t_{cr}$):

$$I_s(t) = (1 - R(\bar{S}_{cr}))I_0(t) \exp(-\alpha_p h(t)) \tag{68}$$

Here $h(t) = z_s(t)$ refers to the ablated depth at time $t$, and $\alpha_P$ refers to the Lagrange extinction coefficient of the plume (extinction coefficient of the plume recalculated per ablated depth). Here we neglect the possible influence of plume on the reflection coefficient. From eqs 64 and 68, we obtain the ordinary differential equation:

$$V = \frac{dh}{dt} = \frac{I_0(t) \exp(-\alpha_p h)(1 - R(\bar{S}_{cr}))}{\hbar\omega\kappa_{ph}}; \quad h(t_{cr}) = 0 \tag{69}$$

Integration of eq 69 yields the etch depth, $h_e$, per single pulse as a function of laser fluence:

$$h_e = \frac{1}{\alpha_p}\ln\left(1 + \frac{\alpha_p(\Phi - \Phi_{th})(1 - R(\bar{S}_{cr}))}{\hbar\omega\kappa_{ph}}\right) \quad (70)$$

Let us consider several special cases of this formula. Thus, if reflection coefficient is not practically influenced by the modification process, $R(\bar{S}) = \text{const} = R$, then (see eq 67)

$$\bar{S}_{cr} = \Phi_{th}(1 - R); \quad \kappa_{ph} = \frac{1}{\hbar\omega}\int_0^{\Phi_{th}(1-R)}\alpha(\bar{S})d\bar{S},$$

and if in addition $\alpha(\bar{S}) = \text{const} = \alpha$, then

$$\kappa_{ph} = \frac{\Phi_{th}(1 - R)\alpha}{\hbar\omega}$$

and (eq 70) becomes:

$$h_e = \frac{1}{\alpha_p}\ln\left(1 + \frac{\alpha_p(\Phi - \Phi_{th})}{\alpha\Phi_{th}}\right)$$

This equation coincides with the formula obtained in ref 30.

Let us consider now multiple-pulse ablation kinetics. If $\Phi > \Phi_{th}$, then at the end of the first pulse we have at the boundary $\bar{S} = \bar{S}_{cr}$. If $\Phi < \Phi_{th}$ then we have no ablation at all for the number of pulses less or equal to $\langle\Phi_{th}/\Phi\rangle$, an integer part of the number $\Phi_{th}/\Phi$, (incubation) and then, after the next pulse, we have $\bar{S} = \bar{S}_{cr}$ at the boundary. Thus, in both cases each pulse, which ordinal number is greater than $\langle\Phi_{th}/\Phi\rangle + 1$, *will etch absolutely the same depth*, which can be easily found from eq 69 with the initial condition $h(0) = 0$. This yields the resulting ablated depth per such pulse:

$$h_e = \frac{1}{\alpha_p}\ln\left(1 + \frac{\alpha_p\Phi(1 - R(\bar{S}_{cr}))}{\hbar\omega\kappa_{ph}}\right) \quad (71)$$

If one irradiates material with an amount of pulses much greater than $\langle\Phi_{th}/\Phi\rangle + 1$, then the averaged etch depth per pulse, which usually is calculated as the resulting depth divided by the number of pulses, can be estimated using eq 71. If $R(\bar{S}) = \text{const} = R$ and $\alpha(\bar{S}) = \text{const} = \alpha$, eq 71 becomes:

$$h_e = \frac{1}{\alpha_p}\ln\left(1 + \frac{\alpha_p\Phi}{\alpha\Phi_{th}}\right) \quad (72)$$

The "photochemical law" (eq 1) is often used for interpreting the data on laser ablation kinetics:

$$h_e = \frac{1}{\alpha_{eff}}\log\left(\frac{\Phi}{\Phi_{app.th}}\right) \quad (73)$$

Here $\alpha_{eff}$ is the effective absorption coefficient and $\Phi_{app.th}$ is the apparent threshold. Equation 71 follows this law at high fluences. Here $\alpha_{eff} = \alpha_P$ and $\Phi_{app.th} = \hbar\omega\kappa_{ph}/\alpha_P(1 - R(\bar{S}_{cr}))$ in the case of eq 72 $\Phi_{app.th} = \Phi_{th}\alpha/\alpha_P$. For smaller, fluences eq 72 deviates from the logarithmic law, with $h$ tending to zero when $\Phi \to 0$. That corresponds qualitatively to the behavior of the kinetics curve obtained in ref 82 for laser ablation of PMMA and Teflon at 125 nm.

For small fluences the kinetics curve predicted by eq 71 follows the linear law:

$$h_e \cong \frac{\Phi(1 - R(\bar{S}_{cr}))}{\hbar\omega\kappa_{ph}} \quad (74)$$

or in case (eq 72):

$$h_e = \frac{\Phi}{\alpha\Phi_{th}} \quad (75)$$

## F. Examples. The Single-Step Model

Let us once again consider the simplest photochemical eq 6, where A stands for the element of the initial material, and B refers to the product of photochemical reaction. In our case, this transition corresponds to chain breaking with simultaneous creation of byproducts, which change the optical properties of the material. For example, it can be direct chain breaking of main polymer chain which is accompanied by the creation of unsaturated C═C bonds near the newly developed ends of polymer chain (see, e.g., ref 84). It is known that the chain breaking process due to irradiation of polymers by UV and VUV photons is often accompanied by a significant change of absorption.[84−86] It can be either darkening or bleaching. The kinetics of modification caused by eq 6 is addressed by the set of eq 7. We rewrite this set in an equivalent form.

$$\frac{\partial N_B}{\partial t} = \frac{\eta_A\sigma_A}{\hbar\omega}(N_0 - N_B)I \quad (76)$$

$$\frac{\partial I}{\partial z} = -(\sigma_B N_B + \sigma_A(N_0 - N_B))I \quad (77)$$

Here $N_B$ stands for the number density of broken bonds, $N_0$ being the number density of initial bonds, and $N_0 - N_B$ being the number density of surviving bonds. $\sigma_A$ refers to the absorption cross-section of initial material recalculated per number density of initial bonds. $\sigma_B$ refers to the absorption cross-section of products of photochemical reaction recalculated per number density of broken bonds. $\eta_A$ stands for the quantum yield of photochemical bond scission. $N_B = N_{cr}$ stands for the critical number density of broken bonds providing ablation. We apply the mathematical approach developed in the previous section. We choose $N_B$ as an $S$ variable, $S = N_B$, then

$$\Psi = \frac{\eta\sigma_A}{\hbar\omega}(N_0 - N_B); \quad \alpha = \sigma_B N_B + \sigma_A(N_0 - N_B);$$

and then

$$\kappa_{ph} = \int_0^{N_{cr}}\frac{\alpha(N_B)}{\Psi(N_B)}dN_B = \frac{N_{cr}}{\eta_A}(1 + \tilde{\gamma}) \quad (78)$$

Here

$$\tilde{\gamma} = \beta\left[\frac{1}{\delta}\ln\left(\frac{1}{1-\delta}\right) - 1\right], \quad \beta = \frac{\sigma_B}{\sigma_A} \text{ and } \delta = \frac{N_{cr}}{N_0}$$

Equation 71 now looks as follows (if we suppose that $R(N_B) \approx \text{const} = R$):

$$h_e = \frac{1}{\alpha_P}\ln\left[1 + \frac{\eta_A \alpha_P \Phi(1-R)}{\hbar\omega N_{cr}(1+\tilde{\gamma})}\right] \tag{79}$$

For small $\delta$, $\delta \to 0$, $\tilde{\gamma} \to 0$, and $\kappa_{ph} \approx N_{cr}/\eta_A$; therefore, eq 79 for small $\Phi$ (eq 74) comes to the formula of ref 28. However, for real situation $\delta$ appears to be quite close to unity and the effect of modification is significant. Let us estimate typical value of $\kappa_{ph}$. Taking $N_0 \approx 6 \times 10^{21}$ cm$^{-3}$ and $\delta = 1/2$ for $\beta = 1$ and $\eta = 1$ we have $\tilde{\gamma} \approx 1.3$ and $\kappa_{ph} \approx 4 \times 10^{21}$ cm$^{-3}$. If $\beta = 2$ and $\eta = 1$ then $\tilde{\gamma} \approx 1.6$ and $\kappa_{ph} \approx 5 \times 10^{21}$ cm$^{-3}$.

## G. Temperature Estimations

To make the photochemical theory of laser ablation self-consistent, let us estimate the temperature rise, which will occur at the interface during photochemical ablation.[39,40] Really, if this temperature appeared to be high enough either to provide thermal destruction and evaporation of material or to influence significantly the photochemical process, then it would follow that the pure photochemical ablation model is not relevant. Simultaneously, we will estimate the domain of applicability of the above ablation model.

Let us start with the single pulse ablation and perform estimation "from above" of the surface temperature provided that we can neglect the heat diffusion.

In this case the temperature rise, $T$, can be estimated from the equation:

$$\frac{\partial T}{\partial t} = \frac{\alpha(S)I}{c_p\rho} - \sum_{i=1}^{k}\epsilon_i(S)\frac{\Psi_i(S)I}{c_p\rho} \tag{80}$$

Here $c_p$ refers to the specific heat, and $\rho$ is the density of the material. In what follows, for simplicity, we will regard them as constants. Here $\Psi_i(S) \equiv \Psi_i(S_1(S),...,S_n(S))$, $\epsilon_i(S)$ being the endothermic effect of corresponding photochemical transitions. If we introduce the function:

$$\Lambda(S) \equiv \alpha(S) - \sum_{i=1}^{k}\epsilon_i(S)\Psi_i(S) \tag{81}$$

then (eq 80) becomes:

$$\frac{\partial T}{\partial t} = \frac{\Lambda(S)I}{c_p\rho} \tag{82}$$

In fact, in this case the temperature can be regarded as a variable from the set $(S_1,...,S_k)$ (see eq 11) because it obeys an equation of the same type as these photochemical variables.

Using eqs 82 and 16, we can easily find the surface temperature, $T_s$, to be

$$T_s = T_0 + \frac{1}{c_p\rho}\int_{S_0}^{S_{cr}}\frac{\Lambda(S)}{\Psi(S)}dS \tag{83}$$

Here $T_0$ refers to the ambient temperature and we put in zero in the following calculations. If we put all the enthalpies $\epsilon_i$ equal to zero, then, using definition of $\kappa_{ph}$ we obtain the estimation:

$$T_s = \frac{\hbar\omega\kappa_{ph}}{c_p\rho} \tag{84}$$

It should be noted that estimation eqs 83 and 84 are valid for single-pulse ablation. Indeed, while temperature relaxes between pulses due to heat diffusion, variables $S_i$ assumed to be not relaxing.

Let us consider now the case when the heat diffusion is significant. First, we consider stationary ablation when $I_s = \text{const}$ and ablation velocity is also constant, $V = \text{const}$.

The temperature distribution within *the moving reference frame fixed with the ablation front* obeys the equation:

$$\frac{\partial T}{\partial t} = D_T\frac{\partial^2 T}{\partial z^2} + \frac{\Lambda(S)I(z,t)}{c_p\rho} + V\frac{\partial T}{\partial z} \tag{85}$$

Here $z = 0$ corresponds to the interface. $D_T$ is the heat diffusivity. It can be checked directly that from eqs 16 and 20 it follows that

$$\Lambda(S)I(z,t) = -\frac{\partial}{\partial z}(F(S)I) \tag{86}$$

where

$$F(S) = \int_{S_0}^{S}\frac{\Lambda(S')}{\Psi(S')}dS'\Big/\int_{S_0}^{S}\frac{\alpha(S')}{\Psi(S')}dS' \tag{87}$$

It follows from eq 86 that the right part of eq 85 is the full derivative with respect to $z$.

$$\frac{\partial T}{\partial t} = \frac{\partial}{\partial z}\left(D_T\frac{\partial T}{\partial z} + \frac{F(S)I(z,t)}{c_p\rho} + VT\right) \tag{88}$$

With $I_s = \text{const}$ and $V = \text{const}$, the temperature distribution tends to be stationary (see e.g., ref 25). Integration of eq 88 yields the corresponding equation for the stationary temperature:

$$D_T\frac{\partial T}{\partial z} + \frac{F(S)I}{c_p\rho} + VT = 0 \tag{89}$$

If we assume the boundary condition for the temperature to be $\partial T/\partial z = 0$, then eq 89 yields the expression for the stationary value of the surface temperature:

$$T_{st} = \frac{F(S_{cr})I_s}{Vc_p\rho} \tag{90}$$

Substituting the expression for ablation velocity from eqs 63 and 64 yields

$$T_{st} = \frac{1}{c_p\rho}\int_{S_0}^{S_{cr}} \frac{\Lambda(S)}{\Psi(S)} dS \qquad (91)$$

Equation 91 coincides with eq 83. It means that this estimation is good for single-pulse or well-developed ablation. Equation 91 is quite remarkable because $T_{st}$ does not depend on intensity. In fact, when we speak about the photochemical ablation, we assume implicitly that the surface layers are etched *before* they are heated to high temperature. Equation 91 provides a test for such an assumption.

Let us make some estimations. Consider the example of single-step model discussed in previous section. Here $S = N_B$, and

$$\Psi = \frac{\eta_A\sigma_A}{\hbar\omega}(N_0 - N_B); \quad \alpha = \sigma_B N_B + \sigma_A(N_0 - N_B),$$

$$\Lambda = \sigma_B N_B + \sigma_A(N_0 - N_B) - \frac{\epsilon}{\hbar\omega}\eta_A\sigma_A(N_0 - N_B) = \sigma_B N_B + \sigma_A(N_0 - N_B)\left(1 - \frac{\epsilon}{\hbar\omega}\eta_A\right) \qquad (92)$$

Here $\epsilon$ is the endothermic effect of photochemical chain scission and accompanying reactions. Temperature elevation can be expressed as:

$$T_{st} = \frac{1}{c_p\rho}\int_0^{N_{cr}} \frac{\Lambda(N_B)}{\Psi(N_B)} dN_B = \frac{\kappa_{ph}}{c_p\rho}\left(\hbar\omega - \frac{\epsilon\eta_A}{1+\tilde{\gamma}}\right) \qquad (93)$$

If we assume that $\epsilon \geq 0$, then it follows from the fact that $\tilde{\gamma} \geq 0$:

$$\frac{\kappa_{ph}}{c_p\rho}(\hbar\omega - \epsilon\eta_A) \leq T_{st} \leq \frac{\kappa_{ph}\hbar\omega}{c_p\rho} \qquad (94)$$

If, as it was estimated in the previous section, $\kappa_{ph} \approx 4 \times 10^{21}$ cm$^{-3}$ , and if the endothermic effect can be estimated as the bond energy, $E_{bond} \approx 3$ eV, per broken bond, then, for typical value $c_p\rho \cong 2$ J/cm$^3$K, at $\lambda = 125$ nm ($\hbar\omega = 10$ eV), eq 94 yields for $\eta_A = 1$:

$$2.2 \times 10^3 \text{ K} \leq T_{st} \leq 3.2 \times 10^3 \text{ K}$$

This value of the surface temperature between two and three thousand Kelvin is too high to speak about the self-consistent photochemical model. These estimations show that stationary VUV ablation can hardly be considered as pure photochemical if there is no process that makes $\eta_A$ significantly greater than unity (like in chain reactions).

Nonstationary and not adiabatic ablation is comprehensively considered in ref 40.

From the given consideration, one can see that photochemical theory of laser ablation (owing to the direct chain scission process) can be considered in quite a general form. The photochemical modification of the material can be taken into account as well. The formulas obtained can be used, for example, for estimation of VUV laser ablation of polymers.

According to this theory the ablation velocity, after ablation starts, is proportional to the light intensity on the surface, the coefficient of proportionality, $\kappa_{ph}$, being the number density of photons which should be *absorbed* at this particular point to produce critical number density of broken bonds at this point.

For multiple-pulse irradiation this model predicts *logarithmic dependence* of etch depth on laser fluence, if fluence is much higher than apparent threshold, and *linear dependence* for fluences much smaller than apparent threshold.

Temperature estimations show, however, that surface temperature for single pulse or quasi-stationary ablation is small enough only if $\kappa_{ph} < 10^{21}$ cm$^{-3}$.

With larger $\kappa_{ph}$ pure photochemical ablation can be relevant at fluences higher than apparent threshold only with large enough plume extinction coefficient.

It should be noted, however, than for single-pulse ablation, and for high enough fluences for multiple-pulse ablation, this model can hardly be relevant in this pure photochemical variant if there is no physical mechanism that makes quantum yield of photochemical bond breaking significantly greater than unity. It will need consideration of thermally activated processes. These processes can either influence the dark reaction, following the photochemical initiation, such as depolymerization, or change the characteristic of material removal, affecting, for example, the critical number density of broken bonds.

## *III. Photothermal Ablation*

### A. Surface Photothermal Model

Photothermal (or simply thermal) models of polymer ablation can be subdivided into surface and volume ablation models. We start with the surface ablation model, which was successfully applied for fitting the kinetics data on UV ablation of polyimide.[35,36] Originally, the surface ablation model was formulated for laser evaporation of metals,[25] and it can be applied for different kinds of simple solids near ablation threshold. That kind of model is relevant at relatively small fluences when hydrodynamic phenomena, spallation, etc., do not contribute to material removal. With polymers, hydrodynamic motions are hindered because of high viscosity of melts. With thermostable polymers as polyimide ablation crater does not exhibit residue of melting.[7]

For the analysis of thermal ablation, we use a one-dimensional nonlinear heat equation with ablation velocity $V = V(t)$ changing during the pulse. In the moving reference frame fixed with the ablation front:

$$\frac{\partial T}{\partial t} = V\frac{\partial T}{\partial z} + \frac{1}{\rho c_p}\frac{\partial}{\partial z}\left(\kappa\frac{\partial T}{\partial z}\right) + Q \qquad (95)$$

where $\kappa$ is the heat conductivity.

The ablation velocity is approximated by

$$V = V_0 \exp[-E_a/k_B T_s] \qquad (96)$$

and the heat source term $Q$ is given by

$$Q = -\frac{1}{c_p\rho}\frac{\partial I}{\partial z} = \frac{\alpha I}{c_p\rho} \quad (97)$$

In this reference frame $z = 0$ corresponds to the position of the interface and convective term $V\,\partial/\partial z$ appears in the right-hand site of the equations with the time derivative in the left-hand site.

The intensity distribution within the material $I(z,t)$ is governed by the Bouguer−Lambert−Beer equation:

$$\frac{\partial I}{\partial z} = -\alpha I \quad (98)$$

Here $\alpha$ is the effective absorption coefficient. Generally, $\alpha$ should be found from an additional set of equations, but in this section we will treat it as an independently known value. Equation 98 is considered together with the boundary condition

$$I(0,t) = [1 - R(T_s)]I_0(t)\exp[-\alpha_p h(t)] \quad (99)$$

where $I_0(t)$ is input laser intensity, $\alpha_p$ is the Lagrange absorption coefficient of the plume, $R$ is reflection coefficient (which can depend on the surface temperature), and $h(t)$ is the ablated depth

$$h(t) = \int_0^t V(t_1)dt_1 \quad (100)$$

For the energy flux, we employ the boundary condition:[7]

$$\kappa\frac{\partial T}{\partial z}\bigg|_{z=0} = \rho V \Delta H_s \quad (101)$$

Here $\Delta H_s$ is a constant that is close to the difference in enthalpy of solid and gas phases.[7]

The second boundary condition (at infinity) and initial condition are obvious: $T|_{z\to\infty} = T|_{t=0} = T_\infty$. One should use the realistic pulse shape $I_0(t)$. For example, for smooth pulse shape of the excimer lasers one can use approximation:[7]

$$I_0(t) = I_0\frac{t}{t_p}\exp\left[-\frac{t}{t_p}\right] \quad (102)$$

The given problem can be solved numerically, e.g., by finite difference technique with temperature-dependent coefficients—heat capacity, heat conductivity, reflection, absorption coefficient, etc. An efficient method to solve this problem by moment's technique was suggested in ref 36.

The density of solid should be considered with a good accuracy as $\rho$ = const, meanwhile the heat capacity $c$, heat conductivity $\kappa$, and the heat source term $Q$ depend on temperature $T$. These dependencies can be rather complex.

Although some simplifications have been done during the formulation of boundary value problem (eqs 95−102) the model is still acceptable for the *quantitative analysis* of experimental data, while the further simplification, typically, leads to a big decrease in the numerical accuracy of analysis.

In the present form, the model contains nonlinearities and nonstationary effects, which normally can be analyzed by numerical solution with the help of the finite element technique.[87] With the moment method technique[88] which we will use for analysis, the given problem can be efficiently reduced to the system of three coupled nonlinear *ordinary differential equations* practically with a very small loss in accuracy. Solution of the ordinary differential equations, in turn, is appellate to the fast Runge−Kutta procedure, which is a routine part of many mathematical software. Thus, we obtain a fast and realistic (quantitative) simulation of purely thermal effects in laser ablation.[36]

The idea of the "moments method" or "nonstationary averaging" method (see, e.g., ref 88) is close to Galerkin's method to find the approximating solution of the nonlinear problem. This technique, for example, was successfully applied to solve some problems in laser thermochemistry.[89] We applied a similar technique for the analysis of laser ablation problems. The details of the procedure and examination of the method accuracy for particular cases are discussed in ref 90.

The idea of the moment method is quite simple. The exact solution $T = T_{ex}(z, t)$ of the boundary value problem (eq 95−102) should identically fulfill eq 92. We use designation $B[T]$ for the right-hand part of eq 95. Thus,

$$c\rho\frac{\partial T_{ex}}{\partial t} - B[T_{ex}] \equiv 0 \quad (103)$$

If we use some other "test function", i.e., trial solution $T = T_p(z, t)$, instead of $T = T_{ex}$ then the identity of eq 103 will be broken because of the singularity of the Cauchy problem. Nevertheless, we can use the appropriate functions $T_p(z, t)$ for approximation solution if we require that this trial solution will fulfill the "conservation laws" for the moments

$$\frac{dM_n}{dt} \equiv \int_0^\infty dz z^n B[T_p(z,t)] = 0, \text{ where } M_n = \int_0^\infty dz z^n H(z,t) \quad (104)$$

Here $H$ refers to the enthalpy $H(T) = \int_0^T c_p(T_1)dT_1$. The total number of eqs 104 should be equal to total number of unknown time dependent functions within the test function $T_p(z, t)$. This procedure corresponds to minimization of the solution functional $F[T_p(z, t)]$ along the directions $z^n$ within the functional space. If we will use for the trial solution directions of the fastest descent in the functional space, the moment method becomes identical to Galerkin's method.[88]

The difference between the Galerkin and moment methods refers to physics. There is no general algorithm how to chose the trial function. Normally, one chooses the trial solution on the basis of own experience and intuition. In principle, a majority of trial solutions is acceptable. One should know how the fitting functions (unknown functions which one

introduces into the trial solution) will varies vs time. The answer, which yields the Galerkin's method, is that they should vary in such a way that they are as close as possible to the "true solution". Mathematics does not care that some, for example, overall energy conservation law will be broken during the procedure.

The moments method suggests the approximation to the "true solution" is less efficient than the Galerkin procedure. Nevertheless, it warranted that all the conservation's laws which one should fulfill will be fulfilled automatically. Thus, the set of equations with a moment method, normally, has a clear physical sense (of course one should try, in principle, some artificial conservation laws).

Within the example, given in eq 104, the equation for the moment $M_0$ means the average energy balance, while equation for the moment $M_1$ means the local energy balance with respect to some characteristic length $\ell$. A number of important parameters and desirable conservation laws should be introduced from the physical sense of the problem.

Within the discussed problem we will consider two important parameters—the surface enthalpy $H_s(t) \equiv H\,[T_s\,(t)]$ and characteristic length $\ell(t)$ for the enthalpy distribution. These two quantities yield the most important information about the *distribution of internal energy* within the solid, i.e., we believe that this distribution, mainly, control the ablation.

To introduce corresponding moments we first rewrite our boundary value problem for the enthalpy $H$. Thus, eq 95 transforms to

$$\rho\left[\frac{\partial H}{\partial t} - V\frac{\partial H}{\partial z}\right] = \frac{\partial}{\partial z}\left(\kappa\frac{\partial T}{\partial z}\right) - \frac{\partial I}{\partial z}. \tag{105}$$

Within the right-hand part of eq 105 the no transformed functions of the temperature are staying. According to our consideration we introduce two moments

$$M_0(t) = \int_0^\infty H(z,t)dz \text{ and } M_1(t) = \int_0^\infty zH(z,t)dz \tag{106}$$

The mutual relation between $H$ and $T$ is given by ordinary differential equation

$$\frac{dH}{dT} = c_p(T) \quad H|_{T=0} = 0 \tag{107}$$

Thus, the boundary condition (eq 101) can be transformed for the value of surface enthalpy gradient

$$\left.\frac{\partial H}{\partial z}\right|_{z=0} = \frac{V\Delta H_s}{D_{Ts}} \tag{108}$$

Here $D_T = \kappa/c_p\rho$ is thermal diffusivity, index $s$ indicates the surface value, i.e., $D_{T_s} = D_T(T_s)$, etc. Taking into consideration (eqs 107−108), integration of eq 106 yields

$$\rho\frac{dM_0}{dt} = -\rho VH_s - \rho V\Delta H_s + I_s \tag{109}$$

and

$$\rho\frac{dM_1}{dt} = -\rho VM_0 + K_s + \frac{I_s}{\alpha}, \tag{110}$$

where $K_s$ is the integral, typical for the Kirchhoff transform:[7]

$$K_s(t) = \int_0^{T_s(t)} \kappa(T)dT \tag{111}$$

We set the trial solution $H_p(z,t)$ in the following form

$$H_p(z,t) = a(t)\exp[-\alpha z] + b(t)\exp\left[-\frac{z}{\ell(t)}\right] \tag{112}$$

where $a(t)$, $b(t)$, and $\ell(t)$ are some functions of time only. The first term in eq 112 describes the change of the enthalpy distribution with a characteristic scale, related to absorption of radiation, while the second term describes the changes in the enthalpy distribution, related to the heat conduction. The characteristic length $\ell(t)$ plays the same role as a thermal length within the linear heat equation. The amplitudes $a$ and $b$ should be expressed through the surface enthalpy $H_s(t) = H_p(z = 0,t)$ with help of boundary condition (eq 108):

$$a = \frac{1}{1-\alpha\ell}\left[H_s + \frac{V\ell\Delta H_s}{D_{Ts}}\right],$$
$$b = -\frac{1}{1-\alpha\ell}\left[\alpha\ell H_s + \frac{V\ell\Delta H_s}{D_{T_s}}\right] \tag{113}$$

Thus, our trial solution automatically fulfills all the boundary conditions and we can write the equations for unknown functions $H_s$ and $\ell$ using the moment method. Substitution of eqs 112 and 113 into eq 106 yields

$$M_0 = \left(1 + \frac{1}{\alpha\ell}\right)\ell H_s + \frac{V}{\alpha D_{T_s}}\ell\Delta H_s \tag{114}$$

$$M_1 = \left(1 + \frac{1}{\alpha\ell} + \frac{1}{\alpha^2\ell^2}\right)\ell^2 H_s + \frac{V}{\alpha D_{T_s}}\left(1 + \frac{1}{\alpha\ell}\right)\ell^2\Delta H_s \tag{115}$$

Now we can substitute eqs 114 and 115 into eqs 109 and 110 to obtain the set of two ordinary differential equations for $H_s$ and $\ell$. This set of equations can be written in canonical form, but "Mathematica" software[91] permits to performe integration directly from the written form, thus it is not necessary to write big and ugly determinants.

The third equation for the thickness of ablated material (which we need to describe screening effect, see eq 99) is given by

$$\frac{dh}{dt} = V \tag{116}$$

Thus, we transfer the initial boundary value problem into the set of three ordinary differential equations, which we should solve with corresponding initial conditions. The investigation[36,90] shows that

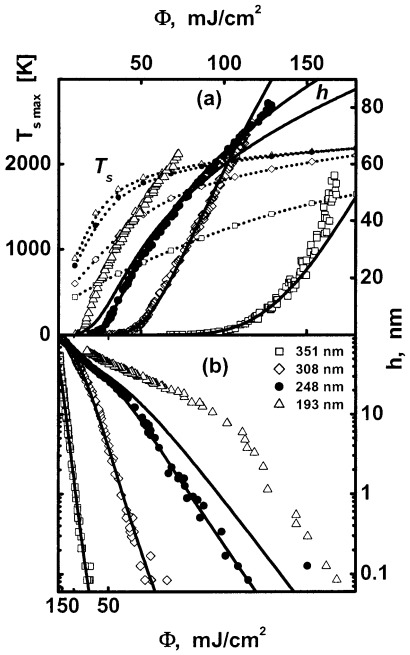


**Figure 5.** Solid curves are results of calculations of laser ablation of polyimide according to thermal model, found by moment's technique.[36] Experimental data are from ref 13. Results are presented in linear (a) and "Arrhenius" (log $h$ vs $1/\phi$) (b) coordinates. The following parameters were used in calculations: $t_p = 6.13$ ns (it corresponds to FWHM 15 ns), $V_0 = 3 \times 10^6$ cm/s, $T_a = 15700$ K $= 1.51$ eV, $T_\infty = 300$ K, $c_p = 2.55-1.59 \exp[(300 - T)/460]$ J/g K, $\kappa = 1.55 \times 10^{-3}(T/300)^{0.28}$ W/cm K, $\rho = 1.42$ g/cm$^3$, $\Delta H_s = 500$ J/g, $\alpha_p = 0.45\ \alpha$, $\lambda = 193$ nm (triangles): A = 0.93, $\alpha = 4.25 \times 10^5$ cm$^{-1}$, $\lambda = 248$ nm (circles): A = 0.88, $\alpha = 3.1 \times 10^5$ cm$^{-1}$, $\lambda = 308$ hm (diamonds): A = 0.89, $\alpha = 10^5$ m$^{-1}$, $\lambda = 351$ hm (squares): A = 0.9, $\alpha = 0.32 \times 10^5$ cm$^{-1}$. In plot (a) maximal temperatures of the surface are shown (dots). The value of temperature is in a good agreement with measured experimentally.[93]

this solution describes well all known analytical solutions, typically, with accuracy 1−3% during the period, comparable with interaction time, i.e., up to ≈3−5 $t_p$ ($t_p$ is duration of laser pulse). The late stage of the temperature evolution, $t \gg t_p$ can be described with less accuracy (≈ 10−30%) but this late stage is not important for the description of ablation.

This solution describes well the influence of the temperature dependencies in $c_p(T)$, $\kappa(T)$, and $R(T)$ and has a lower accuracy for $\alpha(T)$. Within the presented procedure, the temperature dependence in absorption coefficient is taken into account by substitution $\alpha \Rightarrow \alpha_s = \alpha[T_s]$.

Calculations with a thermal model, which take into account all temperature dependencies of parameters, were done in refs 36 and 90. An example of these calculations is shown in Figure 5 for excimer laser ablation of polyimide. One can see that kinetic curves for radiation with 350, 308, and 248 nm are in good agreement with the surface photothermal model. At the same time radiation with 193 nm produces ablation effect strongly different from the thermal model.

One can see that thermal model yields detailed description of the process dynamics. The main problem, however, is that experimentalists typically have no detailed data on the dynamics of the ablation process. Instead of dynamics experimentalist mainly measures integral characteristic, e.g., thickness $h$ of ablated per pulse material versus laser fluence Φ:

$$h = h(\Phi),\ h = \int_0^\infty V(t_1)dt, \Phi = \int_0^\infty I_0(t_1)dt_1 \quad (117)$$

This integral dependence is rather insensitive to many details of the process.[36,61,90] Typically, it contains three parts:

(i) Below-threshold region with $\Phi < \Phi_{th}$ (so-called "Arrhenius tail"), which can be described well by

$$h = A \exp\left(-\frac{B}{\Phi}\right) \quad (118)$$

where A and B are constants;

(ii) Near-threshold region above the ablation threshold, $\Phi > \Phi_{th}$, where the linear dependence is hold (due to overall energy balance)

$$h = \beta(\Phi - \Phi_{th}) \quad (119)$$

(iii) "Screening regime" at $2.5\Phi_{th} < \Phi < 5\Phi_{th}$, where ablation process is strongly influenced by absorption of radiation within the vapor of ablated material; this leads to logarithmic law

$$h = \frac{1}{\alpha_p}\log\left[\frac{\Phi}{\Phi_p}\right], \quad \Phi_p = \frac{B}{\log(\alpha_p A)}. \quad (120)$$

Transitions between different regimes can be described well by the interpolation formula, which can be presented by inverse function $\Phi = \Phi(h)$:[92]

$$\Phi = B \exp[\alpha_p h]\log^{-1}[A/h] \quad (121)$$

In Figure 6 one can see these three typical dependences for the case of excimer laser ablation of polyimide as well as interpolation of experimental data[13] by eq 121.

A weak dependence of integral curves on detailed ablation kinetics means that dependencies $h = h(\Phi)$, presented in hundreds of experimental papers, do not yield sufficient information for the establishing of an ablation mechanism. For this analysis, one needs some additional information. The very informative are data on the dynamics of surface temperature variation, but it is very difficult to measure. Among the few successful examples, we should mention ref 93, where the temperature of polyimide surface during excimer laser ablation was measured near the ablation threshold. Pay attention that this temperature is in good agreement with calculations in Figure 5.

Probably some comment should be made for relatively small activation energy $E_a = 1.51$ eV, used in calculations. This value of the activation energy follows from the analysis of ablation kinetics with fixed intensity and variable pulse duration.[35] This value corresponds to thermo gravimetric measurement for polyimide decomposition.[94] Direct bond

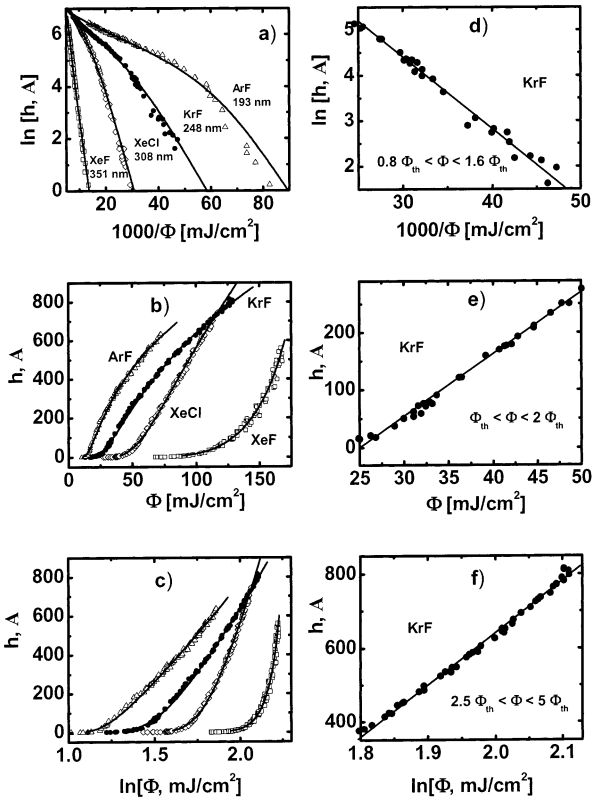


**Figure 6.** Thickness of ablated material (polyimide) per single laser pulse of ArF, KrF, XeCl, and XeF excimer lasers.[13] The same experimental points are presented in different coordinates: "Arrhenius" (log($h$) vs $1/\phi$) (a), linear (b), and logarithmic (c). Solid lines in plots (a), (b), (c) present the best approximation of experimental data by interpolation formula (121). The following values of parameters, obtained by least-squares method, are used (given consequently for four wavelengths − 193, 248, 301, and 351 nm): $A$ = 883547, 29716, 87097, 32562 Å; $B$ = 152.56, 176.13, 370.03, 760.92 mJ/cm$^2$; $\alpha_p = 2 \times 10^5$, $1.22 \times 10^5$, $5.5 \times 10^4$, $-1.9 \times 10^4$ cm$^{-1}$. Plots (d), (e), and (f) are amplified pictures of the regions where experimental data follow "Arrhenius" (118), linear (119), and logarithmic (120) behaviors. These dependencies are presented by straight lines. Zoom pictures are shown for KrF laser but the same behavior can be seen for other wavelengths.

breaking of covalent C−C, C−N, and C−O bonds needs significantly higher energies of 3−5 eV.[95]

## B. Bulk Photothermal Model

In this section, we develop a model, which takes into account the features of polymer-like materials. Polymeric materials are constituted by long macromolecules consisting of sequences of monomers, molecular groups of the same nature. The inherent feature of polymeric materials is the hierarchy of bonds between the molecular groups. There are strong, covalent, bonds connecting adjacent molecular groups of the same chain and weak, molecular, bonds between neighboring groups that belong to different polymer chains. Removal of molecular groups from the surface of material during ablation can proceed through breaking intrachain bonds (covalent). On the other hand, the removal of polymer chain as a whole from the surface is possible as a result of breaking of all weak bonds, which connect this chain with the surrounding material. Of course, if the chain is long enough, this process is suppressed, because the combined energy of weak bonds appears to be greater than a single strong bond. In the presented bulk models, laser ablation proceeds through bulk reaction, which results in the creation of broken bonds (schematic representation of changing strong bonds by weak bonds due to chain scission see in Figure 7). In what follows, we consider the single-step thermally activated reaction A → B. Here A is associated with elements of initial virgin material, while B denotes the reaction products, which in the context of this paper can be attributed to broken bonds. In what follows $N_A$ stands for number density of species A, $N_B$ stands for number density of species B, $n_A = N_A/N_0$ and $n_B = N_B/N_0$ being fractions of unbroken and broken bonds correspondingly. $N_0$ is initial number density of bonds. Thus, chemical kinetics equation for a fraction of broken bonds, $n_B$ reads:

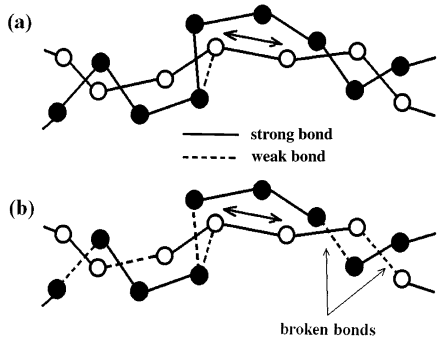


**Figure 7.** Schematic representation of chain breaking process leading to replacement of strong bonds by weak ones. (a) initial material; (b) result of chain scission reaction.

$$\frac{\partial n_B}{\partial t} = V\frac{\partial n_B}{\partial z} + (1 - n_B)k_0 \exp(-E_b/k_B T) \quad (122)$$

Here $k_0$ is a constant, and $E_b$ is the activation energy. Within the bulk model the source term $Q$ in eq 95 contains additionally, compared with eq 97, a term that takes into account the heat effect of the chemical reaction. For nanosecond pulses, we will take

$$Q = \frac{\alpha I}{c_p \rho} - \frac{\Delta H_b N_0 (1 - n_B) k_0 \exp(-E_b/k_B T)}{c_p \rho} \quad (123)$$

Here $\Delta H_b$ is the enthalpy per strong bond, which is broken according to eq 122.

The sum energy of the "weak" bonds between the chain and environment for short enough chains is proportional to its length. In the considered model the ablation mechanism is caused by removal of the sufficiently short polymer chains. Velocity of ablation can be approximated similarly to eq 96, where $E_a$ denotes now the activation energy of removal of a short polymer chain. In the case of degradation of polymer by random chain scission either due to photochemical or photothermal reaction the average chain length is about $\sim 1/n_B$ after several steps.

Neglecting molecular-mass distribution of polymer chains immediately yields eq 96 in which

$$E_a = E_m / n_s \tag{124}$$

Here $n_s$ is the surface value $n_s(t) = n_B(0, t)$. $E_m$ stands for the energy of weak bonds per "monomer". Monomer here means the molecular group between neighboring-along-the-chain bonds, which can be broken. The expression for ablation velocity now reads:

$$V = V_{0m} \exp(-E_m/k_B n_s T_s) \tag{125}$$

Within the approach investigated in this paper we, following refs 43 and 44, employ the equation for ablation velocity (3.30) together with the boundary condition:

$$\kappa(T)\frac{\partial T}{\partial z}\Big|_{z=0} = \rho \Delta H_m V \tag{126}$$

Here $\Delta H_m$ stands for the enthalpy of evaporation of weak bonds per "monomer". The boundary conditions for infinity are obvious, as usual

$$T|_{z\to\infty} = T_\infty,\ n_B|_{z\to\infty} = 0 \tag{127}$$

This Frenkel-Wilson-like bulk photothermal model was formulated in refs 43 and 44.

## C. Stefan-like Bulk Photothermal Model

Equation 125 provides a sharp dependence of ablation rate on the number density of broken bonds at the boundary. In refs 41 and 42 in which the bulk or volume model of laser ablation was comprehensively discussed, the Stefan-like boundary condition was employed instead of eq 125. The ablation starts when the fraction of broken bonds at the surface reaches a certain critical value, $n_{cr}$. The position of the interface thereafter is fixed with this critical number, i.e., the boundary condition reads:

$$n_s = n_{cr} \tag{128}$$

This relation defines the position of the interface, and therefore the velocity $V$, implicitly. Stefan-like condition (eq 128) can be considered as an approximation of eq 125 with very sharp dependence of velocity on fraction of broken bonds at the surface. Another physical meaning of eq 128 can be explained as follows. The interaction of polymer chains can proceed also through topological constrictions, entanglements. There is an averaged number of monomers between the neighbor entanglements, $n_{cr}$, along the chain. If the length of the chain at the surface becomes shorter than this $n_{cr}$ and if $E_m$ can be neglected, we immediately come to the condition (eq 128). In this case enthalpy of evaporation also can be neglected and the boundary condition for the temperature can be written as follows:

$$\kappa(T)\frac{\partial T}{\partial z}\Big|_{z=0} = 0 \tag{129}$$

## D. Stationary Wave Solution in Stefan-like Model

In laser ablation, the understanding of the stationary regime of material removal (with *constant* incident intensity $I_0$ and ablation velocity $V$) is prerequisite for further studies. Its consideration for *surface* models allows one to understand many features of the laser ablation of metals. In general, stationary velocity of the interface is determined by the energy conservation, and temperature is such, that Arrhenius reaction rate is fast enough to maintain this velocity. As a result, velocity is about linear with intensity, while (surface) temperature depends logarithmically on $I$ in almost every *thermal* model. Subsequent mathematical analysis reveals, however, some differences between the surface and volume models.

Below we consider stationary ablation within the model of section IIIC with zero reaction enthalpy $\Delta H_b = 0$ and with temperature independent parameters as it has been done in ref 41. Generalization of this analysis can be found in ref 42.

It is convenient to introduce along with $n_A$ and $n_B$ the variable $b$:

$$b \equiv -\log(1 - n_B) \equiv \log\left(\frac{1}{n_A}\right) \tag{130}$$

Equations 95, 98, 122, 123, 126, and 128 now read:

$$\frac{\partial T}{\partial t} = V\frac{\partial T}{\partial z} + D_T\frac{\partial^2 T}{\partial z^2} + \frac{\alpha I}{c_p \rho} \tag{131}$$

$$\frac{\partial I}{\partial z} = -\alpha I \tag{132}$$

$$\frac{\partial b}{\partial t} = V\frac{\partial b}{\partial z} + k_0 \exp(-E_b/k_B T) \tag{133}$$

$$\frac{\partial T}{\partial z}\Big|_{z=0} = 0;\quad T(\infty) = T_\infty;\quad b(\infty) = 0 \tag{134}$$

$$I(0,t) = I_0(t) \tag{135}$$

$$b(0,t) = -\log(1 - n_{cr}) \tag{136}$$

Here $D_T$ is the heat diffusivity. For stationary solution, we take the solutions that correspond to the constant light intensity $I_0$ and propagate with the constant velocity $V$ = const. The stationary wave solution obeys the eqs 131−136 with all the time derivatives being taken to be zero. In what follows, we take $T_\infty = 0$.

It is easy to find the first integral for stationary solutions (see section IIF). Thus, instead of eqs 131 and 132 we can write:

$$D_T\frac{\partial T}{\partial z} = \frac{I}{c_p \rho} - VT \tag{137}$$

Equations 133−137 yield:

$$V \log\frac{1}{1 - n_{cr}} = k_0 \int_0^\infty \exp\left(-\frac{E_b}{k_B T(z)}\right) dz \tag{138}$$

The integral in the right-hand side of eq 138 can be estimated using the saddle point method. It uses Taylor expansion of $T$ near the surface under the

assumption $T_b/T_s \gg 1$; here we used definition $T_b = E_b/k_B$, $T_s = T$ ($z = 0$):

$$k_0 \exp(-T_b/T) \approx k_s \exp(-z^2/\ell_k^2) \qquad (139)$$

Equations 137 and 134 yield:

$$k_s \equiv k_0 \exp(-T_b/T_s), \quad \ell_k \equiv \ell_T (T_s/T_b)^{1/2},$$
$$\ell_T^2 \equiv -2T_s \left|\frac{\partial^2 T}{\partial z^2}\right|_{z=0} \qquad (140)$$

$$T_s = \frac{I_0}{c_p \rho V} \qquad (141)$$

Equations 131 and 134 yield:

$$\left.\frac{\partial^2 T}{\partial z^2}\right|_{z=0} = -\frac{I_0 \alpha}{D_T c_p \rho}; \quad \left.\frac{\partial T}{\partial z}\right|_{z=0} = 0 \qquad (142)$$

The eq 138 thus becomes:

$$V = \left(\frac{k_0}{\log\frac{1}{1-n_{cr}}}\right)^{2/3} \left(\frac{T_s D_T \pi}{2T_b \alpha}\right)^{1/3} \exp\left(-\frac{2E_b}{3k_B T_s}\right) \qquad (143)$$

Equations 141 and 143 provide a closed set to determine the ablation velocity. This set is much similar to that corresponding to a stationary wave in a simple laser surface evaporation problem. There, along with eq 141 one has the velocity equation in the form, see eq 96:

$$V = V_0 \exp\left(-\frac{E_a}{k_B T_s}\right) \qquad (144)$$

Equation 143 can be approximately represented in the form similar to eq 144

$$V = V_0' \exp\left(-\frac{E_a'}{k_B T_s}\right) \qquad (145)$$

The comparison of eq 144 and 145 leads us to the conclusion that a stationary wave in considered A → B ablation model is similar to the stationary laser surface evaporation wave with *the activation energy which is about two-thirds of the reaction activation energy*, i.e., in eq 145 $E_a' = 2E_b/3$.

More rigorous analysis taking into account temperature dependence of heat conductivity and specific heat and, what is more important, $\Delta H_b \neq 0$ (see ref 42) shows that the expression of stationary velocity on surface temperature in the form eq 145 remains with $E_a'$ slowly dependent on intensity changing from $E_a' = 2E_b/3$ at small intensities to $E_a' = E_b$ at high intensities.

One can see that *for stationary regime* surface evaporation model resembles the model under study in several respects. It is not, however, its limiting case. In particular, it can be shown that in the volume model maximum of temperature is always reached at the surface. Instead of formation of subsurface temperature maximum observed in surface models,[25] the temperature distribution near the surface flattens off. As a result, one can subdivide the $z$-axis into two regions. In the reaction region, absorbed energy goes into the enthalpy of decomposition reaction. In the conduction region, the reaction rate is small and absorption is balanced by changes in temperature. The size of reaction region (for high velocities) is on the order of $1/\alpha$.

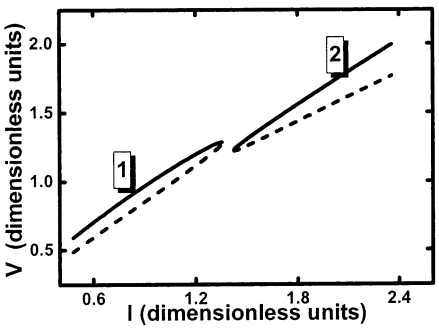


**Figure 8.** A → B → C photothermal model. Stationary ablation velocity, $V$, vs intensity (in dimensionless units). Parameters for the curve 1: $E_B > E_A$; $E_A = 1.5$ eV, $E_B = 3$ eV, $A_1 = 10^{11}$ s$^{-1}$, $A_2 = 10^{13}$ s$^{-1}$. Parameters for the curve 2: $E_B < E_A$; $E_A = 3$ eV, $E_B = 1.5$ eV, $A_1 = 10^{13}$ s$^{-1}$, $A_2 = 10^{11}$ s$^{-1}$. Solid curve − stable branch. Dashed curve − unstable branch. (Reprinted with permission from ref 41. Copyright 1998 Elsevier Science.)

The smoothening of temperature distribution near the surface compared to the surface evaporation model is an important feature of a bulk model. As it is known the temperature distribution near the surface in surface evaporation wave has a maximum beneath the surface. The existence of this maximum is the reason for instability of a plain surface evaporation wave.[25] The absence of such a maximum in a bulk model results in the absence of the reason for instability. That is a bulk model predicts more stable ablation than a surface model.

Let us consider chemical reaction scheme

$$A \rightarrow B \rightarrow C \qquad (146)$$

The second channel: B → C can be interpreted as production of hard-ablated material C such as "glassy" carbon investigated in ref 96. The set of equations describing the chain of reactions of eq 146, will contain eqs 131−135 and 128 completed by the equation for fraction of species B (which we will associate as previously with broken bonds)

$$\frac{\partial n_B}{\partial t} = V\frac{\partial n_B}{\partial z} + n_A k_0 \exp(-E_b/k_B T) - n_B k_1 \exp(-E_c/k_B T) \qquad (147)$$

and for fraction of species A

$$\frac{\partial n_A}{\partial t} = V\frac{\partial n_A}{\partial z} - n_A k_0 \exp(-E_b/k_B T) \qquad (148)$$

In ref 41, we discussed properties of stationary wave solutions of the model A → B → C without taking into account the enthalpies of reactions eqs 131−135, 147, and 148.

It can be seen in Figure 8 (curve 1) that if the activation energy of the bond breaking, $E_b$, is smaller than the activation energy of the following modifica-

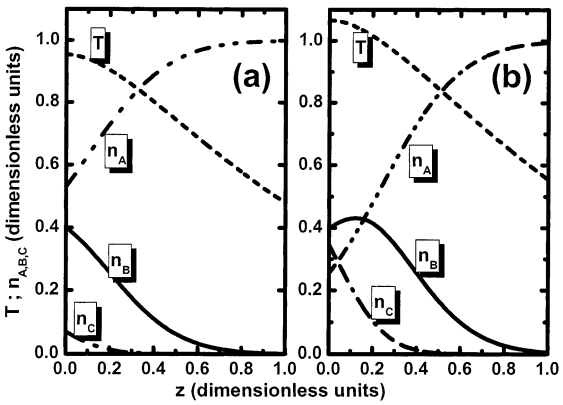


**Figure 9.** Dimensionless coordinate distributions of concentrations and temperature. $n_{cr} = 0.4$. (a) stable branch; (b) unstable branch. (Reprinted with permission from ref 41. Copyright 1998 Elsevier Science.)

tion, $E_c$, then the problem has two stationary solutions at relatively low intensities and no solutions at high intensities. Curve 2 in Figure 8 corresponds to the case in which the bond breaking activation energy is larger than the modification one. Here we have no solution at low intensities and two solutions at high intensities. These interrelations can be understood if we take into account that the higher activation energy process dominates at higher temperatures.

Two branches of stationary solutions demonstrated in Figure 8 are not equivalent. It is illustrated in Figure 9 providing coordinate distributions of temperature and concentrations in stationary waves of different branches. In Figure 9b, the concentration distribution of species B has a maximum at $z \neq 0$. It allows treating this solution as unstable, since the conditions for ablation appeared to be more favorable within the bulk of material than on its surface. Really such a regime cannot be achieved within the considered model starting from any real initial conditions. In Figure 8, the unstable branches are shown by the dashed curves. It should be noted that the surface temperature in the solution of an unstable branch is higher than that of a stable one at the same intensity value.

It has been shown in recent experimental publications[96−98] that during multiple-shot irradiation of polyimide by a KrF excimer laser the increase in etch depth slows down and stops if the fluence is smaller than some "second threshold" one. Several ways to explain these phenomena have been suggested in refs 96−98. The simple model developed above can be treated as one more possible interpretation of these experimental findings.

The absence of stationary solutions can be interpreted as if in these regimes the deep modification causes the ablation front velocity to decrease preventing the achievement of stationary motion. The second threshold here can be assigned to the lower limit of the intensities whereby the ablation velocity is high enough to eliminate the heated region before the deep modification occurs. This assignment is evident from Figure 8 (curve 2).

However, since both the braking bonds and the following deep modification processes are thermally activated, appropriate interrelation between their parameters should exist to provide such a simple picture. Otherwise, the intensity increase may cause the ablation to stop as it can be seen in Figure 8 (curve 1).

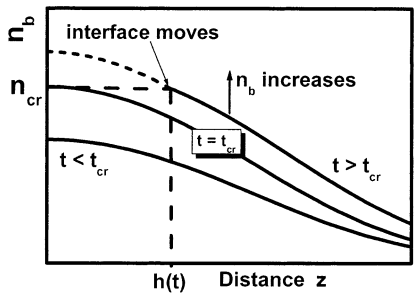


**Figure 10.** Distribution of broken bonds within the material. Before the start of ablation, $t < t_{cr}$, the profile is parabolic near the surface, which leads to an explosive onset of ablation at $t = t_{cr}$. As interface moves $t > t_{cr}$, finite slope of $n_B(z)$ near the surface is formed self-consistently. (Reprinted with permission from ref 42. Copyright 1999 Springer-Verlag GmbH&C.)

## E. Transient Regimes

*Stationary* regimes described in the previous section are seldom reached in nanosecond laser pulses. Besides, they cannot explain near threshold behavior. For this reason we now consider nonstationary regimes, such as the approach to a stationary solution and regimes with the time-dependent intensity. With high fluences screening effects determine the ablation rate for almost *any* ablation mechanism, while near threshold shielding is negligible. Therefore, to discriminate between different ablation models one has to study *near threshold* behavior. In this section, we will assume constant material parameters, zero ablation enthalpy, and Stefan-type condition (eq 128). Consideration of the temperature-dependent parameters usually does not lead to new *qualitative* effects, though it can change the numbers significantly.

Let us consider the laser pulse above ablation threshold. Critical fraction of broken bonds near the surface, $n_{cr}$, is produced at a moment of time $t_{cr}$.

*Before* the movement of the front starts, the profile of broken bonds $n_B$ (or $b$ in (130)) is *parabolic* near $z = 0$, (Figure 10, $t < t_{cr}$), because temperature $T(z)$ and reaction rate have zero derivative at the surface. Thus, at $t = t_{cr}$:

$$b(z) \approx b_{cr} + b''(z = 0)\frac{z^2}{2}; \quad b_{cr} = -\log(1 - n_{cr}) \tag{149}$$

Here prime stands for spatial derivative. After the onset of ablation $n_B$ (and $b$) continue to increase within the volume, and the position of the front in the laboratory system "slides" over the precreated $n_B$ profile in a way that keeps $n_s \equiv n_{cr} = \text{const}$ (Figure 10).

Let us estimate the time $\Delta t = t - t_{cr}$ in which ablation front arrives at the point $z$. At the point $z$, $b$ increases with the rate $\dot{b}(z = 0, t_{cr})$ (the dot stands for time derivative). This is valid with the accuracy about $\Delta t$ and $z^2$, as follows from Taylor expansion.

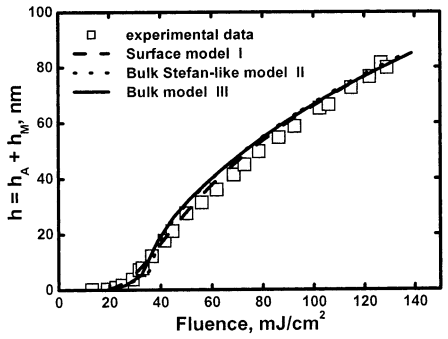


**Figure 11.** Kinetics of laser ablation of polyimide by KrF excimer laser. Experimental mass-loss data are taken from ref 13. (Reprinted with permission from ref 44. Copyright 2002 American Institute of Physics).

Thus, the time needed for $b(z)$ to reach $b_{cr}$ is:

$$\Delta t = -\frac{b''(z=0,\, t_{cr})z^2}{2\dot{b}(z=0,\, t_{cr})} \tag{150}$$

This yields the dependence of ablated depth $h$ on time near the onset of ablation:

$$h(t) = U_0(t - t_{cr})^{1/2}, \quad U_0 = \sqrt{-\frac{2\dot{b}(z=0,\, t_{cr})}{b''(z=0,\, t_{cr})}} \tag{151}$$

Here $U_0 = \text{const}$ and can be estimated as follows; see details in ref 42:

$$U_0 \approx \left(\frac{2D_T}{\exp(-\alpha^2 D_T t_{cr})/\mathrm{erfc}\sqrt{\alpha^2 D_T t_{cr}} - 1}\right)^{1/2} \tag{152}$$

Square root dependence in eq 151 leads to an infinite velocity at the initial moment (explosive onset of ablation):

$$V = \frac{U_0}{2(t - t_{cr})^{1/2}}. \tag{153}$$

The derivative $\partial n_B/\partial z(z = 0) \neq 0$ anymore, but becomes negative, and, finally (for the constant intensity) approaches its stationary value (Figure 10, $t > t_{cr}$).

With $U_0$ from eq 152 the resulting time derivative $\dot{T}_s = \dot{T}_s$ ($h \equiv 0, t_{cr}$) is equal to zero, i.e., $T_s \approx$ const. This explains why $T_s$ stabilizes quickly. It has the tendency to remain constant even for $I(t) \neq$ const.

Figure 12 shows differences in the onset of ablation in the volume Stefan-like model (II) and surface model (I). Initial heating stages are similar. In the volume Stefan-like model ablation starts sharply and the velocity is initially singular. Such an "explosion" may be responsible for the acoustic signal, which was frequently used to determine ablation onset.[99] In the surface model, ablation starts earlier in an Arrhenius-type fashion and velocity does not significantly exceed its stationary value. The differences are most pronounced *near the onset*. In the later stages, both models predict similar quasistationary regimes.

Differences between the volume and the surface model are even more pronounced for near threshold

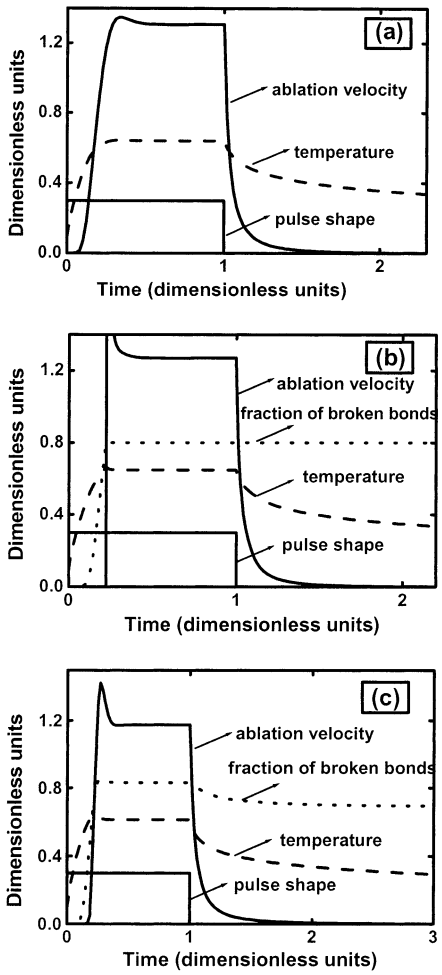


**Figure 12.** Dynamics of laser ablation for rectangular pulse. Absorption by plume is absent. Pulse fluence is significantly above the threshold. (a) surface model I, (b) Stefan-like model II, (c) bulk model III. (Reprinted with permission from ref 44. Copyright 2002 American Institute of Physics).

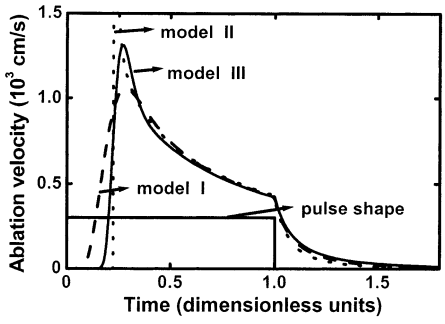


**Figure 13.** Dynamics of laser ablation with high plume absorption. (Reprinted with permission from ref 44. Copyright 2002 American Institute of Physics).

ablation by short pulses with variable intensity. With the *volume* mechanism broken bonds are accumulated within the bulk during the time when the material is hot. Thus, thermal history of the specimen becomes important. With $\Phi \approx \Phi_{th}$, ablation starts *after* the laser pulse and *after* the maximum temperature $T_m$ is reached at $t = t_m$ (Figure 14b). Formally, with $\Phi \rightarrow \Phi_{th} + 0$, the burst of ablation occurs at $t \rightarrow \infty$. With the *surface* model the onset of ablation is smooth, the maximum of ablation velocity coincides with the maximum of surface temperature and the

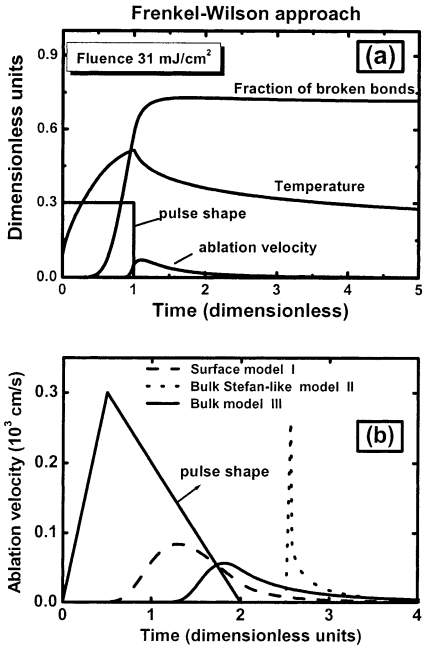


**Figure 14.** Dynamics of laser ablation with near-threshold fluence. (a) Rectangular laser pulse. Maximum of ablation velocity according to bulk model III occurs after the end of the pulse. (b) Triangular laser pulse. Ablation dynamics shown in this picture corresponds to the same fluence for all three models. (Reprinted with permission from ref 44. Copyright 2002 American Institute of Physics).

velocity remains always small. For the *volume* model, despite small total ablated depth, the maximum value of velocity is very big (singular) even near the threshold.

Let us discuss the fluence dependence of the single-pulse near threshold total ablated depth and the threshold fluence. *Near the threshold*, ablation does not influence the temperature and the reaction rate. Therefore, one can assume, that the profile *b(z)*, which is parabolic near $z = 0$:

$$b(z) \approx (b_{cr} + \Delta b)(1 - z^2/\ell_k^2(t_m)) \qquad (154)$$

is created near $t \approx t_m$ when the reaction rate has a sharp maximum. Here $t_m$ is the moment of time when the surface temperature has its maximum, $l_k$ is introduced in eq 140. Afterward, material with $b(z) > b_{cr}$ is ablated. Therefore, *total* ablated depth per pulse $h_e = h\ (t = \infty)$ is:

$$h_e \approx \left[\frac{\Delta b}{b_{cr}}\right]^{1/2} \ell_k(t_m) \qquad (155)$$

To relate $h_e$ to the parameters of the laser pulse, one can apply the saddle point method near $t_m$, which yields[42]

$$h_e \approx \left(\frac{\Phi - \Phi_{th}}{\Phi_{th}}\right)^{1/2} \qquad (156)$$

## F. Kinetics and Dynamics of Ablation. Depletion of Species and Real Ablation

In this section, we compare predictions of different photothermal models regarding kinetics and dynamics of laser ablation by UV nanosecond pulses. We consider three models:[43,44]

I. Surface photothermal model formulated in section IIIA.

II. Bulk photothermal Stefan-like model (section IIIC).

III. Bulk photothermal Frenkel-Wilson-like model (section IIIB).

The above sets of partial differential equations were solved numerically using finite difference methods of solving quasilinear parabolic differential equations.[100] Implicit schemes complemented by the sweeping method of solving corresponding sets of linear algebraic equations were used. When treating nonlinearities (temperature-dependent parameters and ablation velocity that is a function of temperature) a combination of linear and nonlinear schemes were used; in latter cases the iteration procedures were applied. The most important point is the use of variable steps in spatial grid. The distribution of steps should take into account the different spatial scales involved: absorption length and heat diffusion length. When considering ultrashort laser pulses (USLP) different temporal scales, namely, pulse duration, relaxation times, heat diffusion time were taken into account. Thus, in this case variable steps in time were used. These steps are small enough during laser pulse, somewhat greater during relaxation time, and relatively big during heat diffusion. When treating the Stefan-like problem, we essentially employ the relation:

$$V = -\left.\frac{\partial n_B}{\partial t}\right|_{z=0} \Big/ \left.\frac{\partial n_B}{\partial z}\right|_{z=0}$$

This relation is valid after ablation starts. Codes used for calculations in this section can be downloaded from the site http://www.iapras.ru/structure/optics/div330/lab332/reslines.asp.

First we compare ablation kinetics, i.e., the dependence of ablated depth on fluence per pulse. We consider the experimental data on mass-loss kinetics of polyimide irradiated by KrF excimer laser.[13] These data demonstrate "Arrhenius tails" near ablation threshold. Bulk models II and III cannot explain these tails, if we assume layer-by-layer ablation as the only reason for mass-loss. However, it has been understood in refs 101 and 42 that these tails originate from the depletion of volatile species. These volatile species result from the same bulk reaction A → B. This reaction breaks the bonds, destroys polymer chains, and may simultaneously create trapped volatile species. Below ablation threshold, the volatile species result in a mass loss, which requires out-diffusion of trapped species and occurs on the microsecond or even millisecond time scale. As volatile species and broken bonds are produced in a pyrolytic reaction, this results in an Arrhenius tail. Above the threshold, the volatile species leave the material together with the ablation products. When ablation ceases some of the volatile species still exist below the surface and leave the material later. This results in an additional mass loss, *M* (per unit area), which does not contribute necessarily to the ablated (crater) depth. The above picture is not in

contradiction with recent experimental spectroscopic findings.[102] $M$, which is due to the depletion of species, is proportional to the number of broken bonds left within the material after ablation. Because these species do not diffuse on the ns time scale, their spatial distribution repeats that of the broken bonds and $M$ can be calculated as:

$$M = m_v N_0 \int_0^\infty n_B(z)dz \qquad (157)$$

where $N_0$ is the total concentration of virgin bonds, and $m_v$ is the mass of volatile products produced per broken bond. To compare the theoretical curves with experimental data on mass-loss kinetics we introduced the equivalent "depth" $h_M$ related to $M$,

$$h_M \equiv \frac{M}{\rho} = \frac{m_v}{m_t}\int_0^\infty n_B(z)dz \qquad (158)$$

the ablation depth $h_A$ and also the total effective "depth" $h = h_A + h_M$. Here $m_t$ is the initial mass per virgin bond, and $\rho = m_t N_0$.

We carried out the calculation of laser ablation kinetics by nanosecond pulses with mass-loss. Figure 11 shows the mass-loss kinetics curve for all three considered models in comparison with the experimental data of ref 13 on KrF laser ablation of polyimide. The parameters used are listed in Table 2. It should be noted that the set of parameters for each model could be changed somehow without damaging the quality of fitting shown in Figure 11. It is seen from these curves that it is really hard to distinguish between the models using only data on ablation kinetics by nanosecond pulses.

It should be noted, however, that the ablated depth measured by profilometry (optical interferometer, mechanical stylus,[103] atomic force microscope (AFM)[104]) shows that ablation starts *sharply* at fluence $\Phi = \Phi_{th}$. Similar conclusions can be drawn from reflectivity[105] or acoustic response measurements.[99]

The bulk models provide the key to the explanation of such discrepancy between mass-loss and profilometry experiments. It implies that the latter measure real layer-by-layer ablation whereas the former takes into account the mass-loss provided by depletion of volatile species as well. This picture should rather serve as a guideline for the experiments, which target to determine the discrepancy between the mass-loss and profile measurements in single pulse ablation.

The mass-loss from the bulk of material may influence the surface morphology even below threshold. In polymers with flexible chains, such as PMMA, this may result in essential decrease of thickness of thin polymer film due to free volume relaxation.[77] In polymers with hard chains, such as polyimid, this relaxation should be hindered. On the other hand, with polyimid such phenomena as "hump" and "dent" formation are observed.[106] They impede the AFM measurements of ablation kinetics near the threshold.

Let us now consider the dynamics of ablation, i.e., the time dependence of surface temperature, and ablation velocity. As it was discussed above, differences between ablation dynamics predicted by the surface photothermal model and the Stefan-like bulk model are as follows:

(i) The sharp, singular onset of ablation predicted by model II with pulses well above ablation threshold instead of relatively smooth time dependence of ablation velocity demonstrated by model I.

(ii) With laser pulse with fluence close enough to the ablation threshold, ablation governed by model II starts after the laser pulse, but according to model I, ablation will start no later than the onset of the maximum of surface temperature, which corresponds to the end of the rectangular pulse, and occurs even before the end of the pulse for more realistic shape of a laser pulse.

The aim of this section is to check how these features of the bulk model remain for a more realistic model III. In Figure 12, we neglect the absorption by the plume ($\alpha_p = 0$). It is seen that the onset of laser ablation for a rectangular pulse is sharp enough with model III as well. The surface temperature tends to its stationary value from above in contrast to the prediction of the surface model I. Of course, in model III there is no singularity as it occurs with model II. The difference in dynamics between surface and bulk ablation (model III) is less pronounced if the absorption by the plume is strong enough as it takes place for polyimide (see Figure 13 and Table 2).

**Table 2. Parameters Used in Calculations**[a]

| models parameters | photothermal surface model | bulk model |
|---|---|---|
| activation energy (surface) | | |
| $E_a$, eV | 1.5 | |
| $E_m$, eV | | 0.7 |
| surface sublimation | | |
| enthalpy $\Delta H_s$, J/g | 900 | |
| $\Delta H_m$, J/g | | 650 |
| surface preexponential | | |
| $V_0$, cm/s | $3 \times 10^6$ | |
| $V_{0m}$, cm/s | | $1.1 \times 10^5$ |
| volumetric activation energy $E_b$, eV | | 1.5 |
| volume preexponential $k_0$, $s^{-1}$ | | $3.57\times10^{12}$ |
| volumetric reaction enthalpy $\Delta H_b$, J/cm$^3$ | | 2000 |
| fraction of volatile species | | 0.32 |
| critical fraction of broken bonds $n_{cr}$ (model II) | | 0.8 |
| ambient temterature $T_\infty$, K | 300 | 300 |

| parameters polyimide Kapton H, $\lambda$= 248 nm | value |
|---|---|
| density $\rho$, g/cm$^3$ | 1.42 |
| specific heat $c_p$, J/g K (ref 36) | $2.55-1.59 \times \exp[(300 - T)/460]$ |
| thermal conductivity $\kappa$, W/cm K (ref 36) | $1.55 \times 10^{-3}\times (T/300)^{0.28}$ |
| thermal diffusivity $D_T$, cm$^2$/s | $\kappa/c_p \rho$ |
| reflection coefficient $R$ | 0.1 |
| absorption coefficient $\alpha$, cm$^{-1}$ | $3.2 \times 10^5$ |
| screening coefficient $\alpha_p$, cm$^{-1}$ | $1.4 \times 10^5$ |
| number density of chromophores in a medium $n_0$ cm$^{-3}$ | $6 \times 10^{21}$ |
| relaxation times of excited states | |
| $t_{21}$, ps | 30 |
| $t_{32}$, ps | 70 |
| $\sigma_{23}/\sigma_{12}$ | 1 |

[a]Reprinted with permission from ref 44. Copyright 2002 American Institute of Physics.

According to the model II, ablation starts after the end of the pulse, when laser fluence belongs to some interval of fluences just above the ablation threshold. Of course, with model III this feature should remain (see Figure 14a). But our calculations show that this interval becomes shorter for model III compared to model II. It is illustrated in Figure 14b, where the dynamic curves of ablation for all the models correspond to the same value of fluence. Figure 14b illustrates that at fluence, at which model II predicts the onset of ablation *after the end of the pulse*, ablation starts *within the pulse* according to model III. Moreover, our calculations with parameters listed in Table 2 show that with model III this interval of fluences is so short that hardly can be resolved experimentally, especially for pulse shape close to that of excimer laser.

In conclusion, it can be mentioned that the features of ablation dynamics predicted by the bulk model of laser ablation remain in model III. Nevertheless, it should be noted that the smoothening provided by eq 125 of model III, compared with the Stefan-like condition (eq 128), makes it difficult to distinguish between the bulk and surface mechanisms by using experimental data on ablation kinetics and dynamics with nanosecond pulses. We show below that it can be done using experimental data on ultrashort laser ablation.

## *IV. Subpicosecond Ablation*

### A. Bulk and Surface Models

The laser ablation by ultrashort laser pulses (USLP) offers potentials for precise treatment of materials. This phenomenon has recently attracted the attention of many investigators since it allows elucidating features of laser−material interactions on the subpicosecond time scale.[107−111]

It is perceived now that the threshold of USLP ablation of transparent dielectrics coincides with the onset of avalanche or multiphoton ionization.[109−111] It is not so evident for highly absorbing dielectrics because ablation due to heating of a material in this case can occur at fluence which is smaller than that needed for avalanche or stepwise ionization development.

With ultrashort laser pulses, we cannot employ equation of section III with $\alpha = \text{const}$. We have to consider the transient response of a media. We shall assume that radiation is absorbed in a material by chromophore groups (chromophores),[95] i.e., that the first electronic transition occurs in a bound state, which is typical of polymers. Since an important feature of such a response is the saturation of energy levels, the absorption of radiation in a dielectric will be described by multilevel models of this medium and we shall take into account stimulated emission and nonradiative relaxation. A set of rate equations for the populations of the energy levels within the three-level model shown in Figure 15 reads:

$$\frac{\partial n_1}{\partial t} = V\frac{\partial n_1}{\partial z} - \frac{\sigma_{12}}{\hbar\omega}I(n_1 - n_2) + \frac{n_2}{t_{21}} \qquad (159)$$

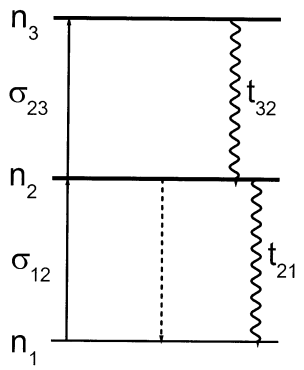


**Figure 15.** Schematic of electronic structure of chromophores; $n_1$, $n_2$, and $n_3$ are populations of the corresponding levels; $n_0$ is the number density of chromophores in the medium; $\sigma_{ij}$ are the cross sections of the transitions; $t_{21}$, $t_{32}$ are the nonradiative relaxation times of electronically excited states.

$$\frac{\partial n_2}{\partial t} = V\frac{\partial n_2}{\partial z} + \frac{\sigma_{12}}{\hbar\omega}I(n_1 - n_2) - \frac{\sigma_{23}}{\hbar\omega}In_2 - \frac{n_2}{t_{21}} + \frac{n_3}{t_{32}} \qquad (160)$$

$$n_1 + n_2 + n_3 = n_0 \qquad (161)$$

Here $n_1$, $n_2$, and $n_3$ are populations of the corresponding levels; $n_0$ is the number density of chromophores in a medium (in our calculations we take $n_0 = N_0$); $\sigma_{ij}$ are the cross-sections of corresponding transitions; $t_{21}$, $t_{32}$ are the nonradiative relaxation times of electronically excited states. In eq 160, the stimulated emission is ignored at the transitions between the third and the second levels. The transition to the third level can correspond to photoionization of chromophores from the excited state. As it was discussed in refs 112 and 113, this model of a medium response allows fitting experimental data on two-pulse ablation of polyimide. The absorption coefficient will be expressed as:

$$\alpha = \sigma_{12}(n_1 - n_2) + \sigma_{23}n_2 \qquad (162)$$

The heat source term in eq 95 should be rewritten as follows:

$$Q = \frac{\hbar\omega}{\rho c_p(T)}\left(\frac{n_2}{t_{21}} + \frac{n_3}{t_{32}}\right) - \frac{\Delta H_b N_0(1 - n_B)k_0 \exp(-E_b/k_B T)}{c_p\rho} \qquad (163)$$

For surface photothermal model we should take eq 163 with $k_0 = 0$. In numerical calculations below, we consider Gaussian USLP with pulse duration 500 fs.

### B. Kinetics of Single- and Two-USLP Ablation

The dependence of ablated depth on laser fluence predicted by both surface photothermal model I and bulk photothermal model III of the previous section III is studied in ref 44. The characteristic features are as follows:

(i) The bulk ablation starts sharply when fluence approaches the threshold value, whereas the surface ablation exhibits Arrhenius tail near ablation threshold.

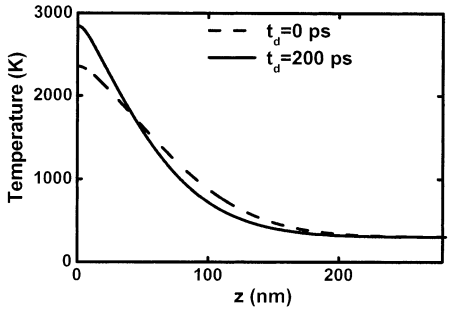


**Figure 16.** The dependences of the temperature on the coordinate directed into the material, calculated for $t_{21}$, $t_{32} < t \ll t_{D_T}$ and without moving interface ($t_{D_T}$ is the characteristic heat diffusion time). (Reprinted with permission from ref 44. Copyright 2002 American Institute of Physics).

(ii) After the threshold, the kinetics curve is almost linear in the case of surface model whereas for bulk mechanism it follows square root law investigated in ref 42 (see section IIIE).

Despite these differences, the kinetics curves are too close to each other to be reliably distinguished in experiments. Now we consider the effect of two USLP with a variable delay time, $t_d$, between them. Zero delay corresponds to the impact of a single pulse with doubled energy. The effect of two successive USLP can be characterized by the dependence of the thickness of the ablated layer, $h$, on the delay time $t_d$ between these pulses. Hereafter this dependence, $h(t_d)$, will be referred to as delay curve. Experimentally, this curve has been obtained for polyimide in ref 107; theoretically, for a surface photothermal model, it has been analyzed in refs 112 and 113. Following ref 107, we consider the situation when laser fluence of one single pulse is smaller than the ablation threshold, whereas the fluence of a doubled pulse (zero delay between the pulses) exceeds the threshold. In this case, ablation starts after the end of the second pulse. In the qualitative analysis given below, we shall assume, to be specific, that (unless otherwise stated) ultrashort pulses bleach effectively the investigated medium. Such bleaching, in turn, results in different localization of the absorbed energy of two ultrashort pulses with different delays between them when the delay time is less than a characteristic heat-diffusion time. The medium is heated after the relaxation of all the electronically excited states. It is important that an increase in the delay between two USLPs reduces the saturation of the levels, since some of electrons drop from an electronically excited state to the ground state before the arrival of the second pulse.

Let us compare the temperature distributions (Figure 16) created by the effect of one doubled pulse (zero delay between the pulses) and by two pulses with a delay exceeding the electronic relaxation time in the medium neglecting heat diffusion. These distributions are characterized by two important parameters: the characteristic spatial scale of the heated region and the surface temperature. The region heated by one doubled pulse is larger than that produced by the effect of two pulses, but the surface temperature in this case is lower. One can ask in which of these two cases the thickness of the ablated layer will be greater? The answer to this question is not a priori evident. Ablation by ultrashort pulses is governed by the competition between two processes: the heat diffusion and the motion of the ablation front. If the ablation is fast, the heat diffusion can be ignored and the result is a removal of the heated region as a whole. If the ablation is slow, then during the heat diffusion time only a small part of the region heated by radiation is removed.

Let us illustrate that with the example of a two-level model ($\sigma_{23} = 0$) and surface photothermal ablation. If the incoming fluence $\Phi > \hbar\omega/\sigma_{12}$, essential saturation occurs. The maximum energy density, which is stored within the bulk of material due to effect of a single USLP, is $w = \hbar\omega n_0/2$. The scale length of energy deposition within the material can be estimated to be $\ell_s = 2\Phi/\hbar\omega n_0$. The maximum temperature value is $T_{max} = T_\infty + n_0\hbar\omega/2c_p\rho$ (we use here temperature independent specific heat) and is independent of fluence. The time scale of heat diffusion is fluence dependent and can be estimated to be $t_{D_T} \sim 2\ell_s^2/D_T$. If $V$ is the ablation velocity, the etch depth, $h$, thus becomes:

$$h \cong t_{D_T} V \cong 8\left(\frac{\Phi}{\hbar\omega n_0}\right)^2 D_T^{-1} V_0 \exp\left(-\frac{E_a}{k_B\left(T_\infty + \frac{n_0\hbar\omega}{2c_p\rho}\right)}\right) \quad (164)$$

If we choose values of the parameters close to those of polyimide: $\rho = 1.42 g/cm^3$, $c_p = 2 J/gK$, $n_0 = 6 \times 10^{21}$ cm$^{-3}$, $\alpha = \sigma_{12} n_0 = 3 \times 10^5$ cm$^{-1}$, $E_a = 1.5$ eV, $V_0 = 10^6$ cm/s and take $\hbar\omega \cong 5$ eV (KrF laser) and $\Phi \cong 50$ mJ/cm$^2$ , we obtain $h \sim 4$ nm whereas $\ell_s \sim 100$ nm. That is $h \ll \ell_s$. When two successive laser pulses each of fluence $\Phi/2$ are applied, the $T_{max}$ increases (approximately two times if $t_d > t_p$), whereas the length scale $\ell_s$ decreases. The resultant etch depth $h$ appears to be closer to the length scale $\ell_s$ and is larger than the etch depth for a single pulse of double fluence. This means that the consideration based on comparison of light penetration lengths does not work here because the material is insufficiently heated. In what follows this kind of behavior of the delay curve will be referred to as the regime of insufficient heating. In this regime, the larger ablated depth corresponds to a higher surface temperature but not to the larger penetration depth. Because $h$ according to eq 164 is proportional to $\Phi^2$, whereas $\ell_s \propto \Phi$, with increasing $\Phi h$ will tend to $\ell_s$. In this case, the ablated depth provided by a big single pulse will be close to the $\ell_s$ and larger than ablated depth provided by two $\Phi/2$ pulses. Here the difference in $\ell_s$ plays a crucial role.

Thus, it seems natural to consider two regimes of laser ablation by ultrashort pulses.[44,112,113]

(i) *Regime with a characteristic heating scale*, when the thickness of the removed layer is governed by the thickness of the heated region of the material, i.e., the ablation is faster than heat diffusion;

(ii) *Regime with insufficient heating*, when the thickness of the removed layer is governed by the

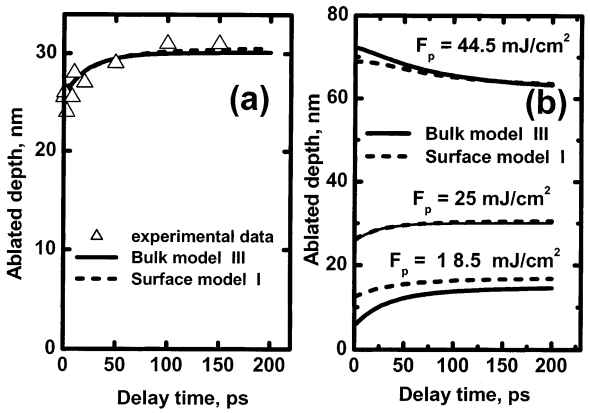


**Figure 17.** (a) The comparison of calculated dependences $h(t_d)$, delay curve, with experimental data[107] for bulk and surface models. Single pulse fluence is $F_p = 25$ mJ/cm$^2$. (b) The dependences of the ablated thickness $h(t_d)$ on the delay time between two ultra short pulses for bulk and surface models and different single pulse fluences.

surface temperature, i.e., ablation proceeds slower than the loss of heat from the absorption region.

As it follows from above, with bleaching the *regime with a characteristic heating scale* provides a greater ablated depth for one doubled pulse than for two separated pulses and a descending delay curve. The *regime with insufficient heating* with bleaching yields an increasing delay curve. These features are opposite for darkening.

It was shown[112,113] that experimental data on 500 fs KrF laser ablation of polyimide[107] with $\Phi = 50$ mJ/cm$^2$ can be qualified as the *insufficient heating regime* with induced bleaching. For the bulk photothermal model, we have similar regimes as for the surface model. It is demonstrated in Figure 17a, in which the above-mentioned experimental data on two-pulse ablation are fitted both by the surface photothermal model and by the bulk photothermal model III. It should be emphasized that the fitting parameters employed are *the same* as for nanosecond pulses. It means that using only data on delay curve it is difficult to distinguish between the models. Really, the delay curve provides information on the dependence of temperature distribution on delay time between USLPs because ablation starts after the setting up of the temperature distribution. These differences in temperature distributions are governed by the material response (transient bleaching or darkening, thermal relaxation time). It should be noted that a lot of relaxation times can be involved in the transient response of the material. It is important, however, that the delay curve allows estimating some averaged thermal relaxation time, which actually governs the setting up of the temperature distribution. This relaxation time corresponds to delay time at which the delay curve saturates. In Figure 17a, this estimation provides the relaxation time of 30−50 ps, which is in correspondence with data of ref 114. The delay curve is less sensitive to the model of ablation. Figure 17b demonstrates the dependence of the delay curve on the fluence of each of the two pulses. It is seen that an increase in single pulse fluence results in change in the shape of the delay curve. This corresponds to the transition from

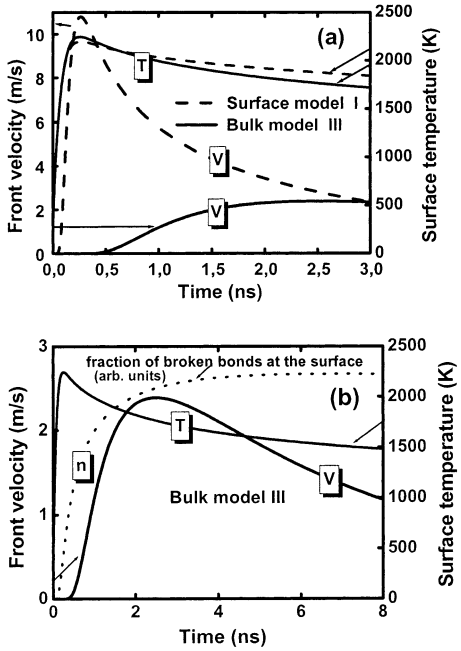


**Figure 18.** Dynamics of laser ablation under the effect of a single 500 fs laser pulse with fluence $F_p = 50$ mJ/cm$^2$ for two ablation models. (a) Ablation front velocity and surface temperature versus time for models I and III. (b) Ablation front velocity, surface temperature and fraction of broken bonds versus time according to the bulk model III. (Reprinted with permission from ref 44. Copyright 2002 American Institute of Physics).

the *insufficient heating regime* to the *characteristic scale regime*. It is valid for both of the considered models. Thus, there is no significant difference between the predictions of the models with respect to kinetics of two- pulse ablation.

## C. Dynamics of USLP Ablation

In contrast to kinetics curves, the dynamics of laser ablation differs drastically for considered models. It is seen in Figure 18a that the maximum ablation velocity for a *surface* model practically coincides in time with the maximum in time dependence of surface temperature whereas the delay time between the maximum heating of the surface of the material and the start of *bulk* laser ablation can be up to an order of magnitude longer than the thermal relaxation time, as shown in Figure 18a,b.

The start of ablation for the surface model is governed by thermal relaxation time, whereas with the bulk model the start of ablation is not governed by thermal relaxation time but rather by the time of thermally activated chemical reaction of polymer chains scission. *The delay time of the start of ablation* after the end of laser pulse for the mechanisms being compared can differ by an order of magnitude.[44] Thus, near ablation threshold the difference in delay time predicted by the considered models is significant and can be experimentally distinguished.

Comparing the predictions of the Frenkel-Wilson bulk model with the predictions of the surface photothermal model and the Stefan-like model, we find out that all the main features of the bulk model, pointed out in ref 42 (sections IIIC−E), remain.

Experiments on kinetics of laser ablation by nanosecond pulses fail to recognize the mechanism of ablation. In ref 42 (section IIIC−E) it was argued that the dynamics of nanosecond ablation differs drastically for the surface and the bulk ablation. Within the present section following ref 44, we show that a more realistic formulation of the bulk model (section IIIB) smoothens the singularities inherent to the Stefan-like model. It leads to the statement that with nanosecond pulses, such factors as deviation from sharp rectangular time shape of the pulse, when considering ablation dynamics near ablation threshold, as well as plume shielding of the incoming radiation for above-threshold ablation, can make it questionable to distinguish between the mechanisms, for example, with parameters close to those of polyimide. With subpicosecond pulses, we show that the investigation of two-pulse ablation kinetics provides information on actual thermal relaxation time almost independently of the mechanisms of ablation. Having this information, one can interpret data on delay time between the end of a single laser pulse and the start of the removal of the material from the surface. In fact, whereas this delay time for the surface model is close to the thermal relaxation time, the delay time for the bulk model can be significantly longer because this time is the time of photothermal reaction providing scission of polymer chains. Thus, a combination of two-pulse and single-pulse ablation experiments with subpicosecond laser pulses provides a way to distinguish between the mechanisms.

The start of ablation can be fixed, for example, using a pump−probe technique.[115−117] The only existing data of relevant time-resolved experiments have been published in ref 107. Two-pulse ablation experiments on subpicosecond ablation of polyimide at 248 nm provided estimation of thermal relaxation time of about 30−50 ps. It was mentioned, however,[107] that within time interval of 200 ps after a single 500 fs pulse with fluence above the ablation threshold there was no evidence of material removal from the surface. From the above analysis, it can be treated as an argument in favor of the bulk model. It should be noted, however, that additional experiments are needed.

## D. Photophysical Ablation

Photophysical model of laser ablation has been suggested in refs 45−47. The main idea is that the activation energy for destruction and elimination from the surface of electronically excited molecules is smaller than the activation energy for the molecules in the ground state. Despite the obvious physical reasons, up to now there is no direct evidence that the photophysical mechanism really works. (It should be noted, however, that recently it has been shown in ref 144 that IR laser ablation of porous Si is strongly enhanced by radiation of the second harmonic. This can be interpreted as a photophysical ablation.)

The aim of the present communication is to investigate the features of photophysical ablation when the material is irradiated by USLP with pulse duration significantly shorter than the electronic energy relaxation time. We compare predictions of photophysical and pure photothermal models to understand the possibility to recognize the photophysical effects.

We consider the effect of USLP on a dielectric, which can be described as a two-level media. The laser frequency is assumed to be in resonance with the electronic transition. We take into consideration that the excited level has a complicated structure, thus the effective bandwidth is larger than the bandwidth of the laser radiation. We assume also that the excited electron changes its energy inside the level in such a way that the transition frequency leaves resonance faster than the pulse duration. Thus, we will not take into account the induced radiation. This approximation is not very important and is made only for the sake of simplicity. We consider laser ablation of such a media within the framework of a surface evaporation model to compare the predictions of surface photothermal and photophysical models.

Both of the models describe the material response in a similar way:

$$\frac{\partial n^*}{\partial t} = V\frac{\partial n^*}{\partial z} + (n_0 - n^*)\frac{I\sigma_{12}}{\hbar\omega} - \frac{n^*}{t_{21}} \quad (165)$$

$$\frac{\partial I}{\partial z} = -I\sigma_{12}(n_0 - n^*) \quad (166)$$

$$\frac{\partial T}{\partial t} = V\frac{\partial T}{\partial z} + \frac{1}{c_p(T)\rho}\frac{\partial}{\partial z}\left[\kappa(T)\frac{\partial T}{\partial z}\right] + \frac{n^*}{t_{21}\rho c_p(T)} \quad (167)$$

with the initial and boundary conditions

$$n^*|_{t=0} = 0,\ T|_{t=0} = T_\infty \quad (168)$$

$$I|_{z=0} = I_0(t),\ n^*|_{z\to\infty} = 0,\ T|_{z\to\infty} = T_\infty \quad (169)$$

Here $I$ is laser intensity, $T$ is the temperature, $n_0$ is the number density of the absorbing groups, $n^*$ is the number density of excited species, $\omega$ is the laser and electronic transition frequency, and $\sigma_{12}$ is the corresponding absorption cross-section. $V$ is the ablation velocity. The coordinate system is fixed with the ablation front. $t_{21}$ is the thermal relaxation time. $\kappa(T)$ is thermal conductivity, and $c_p(T)$ is specific heat.

The difference of photophysical surface model with a surface photothermal model takes place in relation to the velocity of ablation front and in boundary condition for temperature:

$$V = \left(1 - \frac{n_s^*}{n_0}\right)V_0 \exp(-E_a/k_B T_s) + \frac{n_s^*}{n_0}V_0^* \exp(-E^*/k_B T_s) \quad (170)$$

$$\kappa\left.\frac{\partial T}{\partial z}\right|_{z=0} = \left(1 - \frac{n_s^*}{n_0}\right)\rho\Delta H_s V_0 \exp(-E_a/k_B T_s) + \frac{n_s^*}{n_0}\rho\Delta H_s^* V_0^* \exp(-E^*/k_B T_s) \quad (171)$$

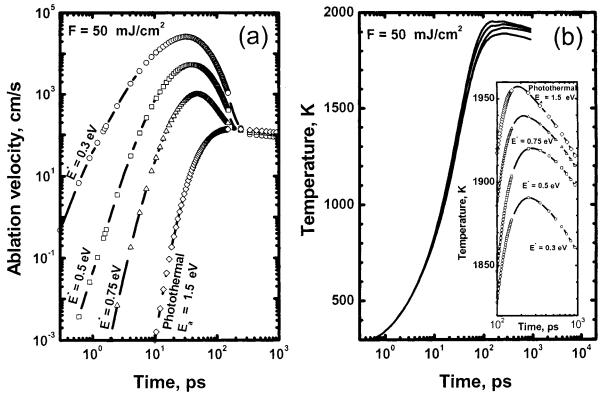


**Figure 19.** Dynamics of laser ablation under the effect of a single laser pulse with fluence 50 mJ/cm$^2$. The photophysical ablation with different $E^*$ and pure photothermal ablation. For all the curves $E_a = 1.5$ eV. (a) Ablation velocity vs time. (b) Surface temperature vs time.

Here $E_a$ and $E^*$ are ablation activation energies for the ground state and the excited state, respectively. The subscript $s$ refers to the ablation front at $z = 0$; $\Delta H_s$ and $\Delta H_s^*$ are the transition enthalpies.

Hereafter in numerical calculations we use the values of parameters close to those of polyimide and for temperature dependencies of thermal conductivity and specific heat we use the expression from ref 36. In what follows, we also use in analytical estimations the averaged values of specific heat, $c_p \approx 2$ J/g K, and heat diffusivity $D_T \approx 10^{-3}$ cm$^2$/s. We take $t_{21} = 30$ ps, $\Delta H_s = 700$ mJ/g, and estimate $\Delta H_s^* = \Delta H_s \times E^*/E$.

Figure 19a exhibits the time dependence of ablation velocity for photothermal model and for photophysical models with different activation energies for elimination of excited species. Since the pulse duration is essentially shorter than relaxation time, ablation starts after the end of the laser pulse. Relaxation of excited species results in an increase of temperature. The ablation velocity, according to a photothermal model, monotonically depends on surface temperature. This leads to a relatively rapid increase in velocity resulting from the temperature rise due to electronic relaxation, this rise being followed by a slow decrease of temperature caused by the penetration of the ablation front into a colder part of the sample and by heat diffusion. The ablation velocity demonstrates another behavior in a photophysical model. The sharp maximum in its time dependence is not connected with the time dependence of the surface temperature but with the decrease of concentration of excited electrons because the ablation velocity is proportional to the concentrations of excited states. When excited states vanish, the velocity of the ablation front reaches its pure photothermal value. This value is slightly less than the correspondent value for a pure photothermal model (see Figure 19a) at the same moment of time. It results from a somewhat smaller value of surface temperature as can be seen from Figure 19b. The reason for that can be understood from Figure 20. Here ablation velocity is displayed versus ablated depth. It is seen that in the considered situation only a small amount of material is ablated photophysically, whereas the main part of ablation proceeds through the photothermal mechanism. The difference between dashed and solid curves in Figure 20 results from the fact that the photophysical ablation front overtakes the photothermal ablation front. Therefore the temperature at the same point of material at the time when the ablation front comes to it, is higher for the photophysical case because of heat diffusion. It follows from Figure 20 that in the considered case the difference between the ablated depths in photophysical and photothermal ablation is essentially due to heat diffusion.

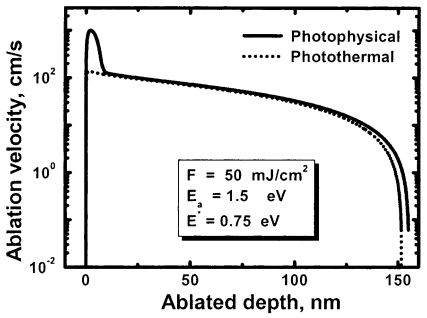


**Figure 20.** Ablation velocity vs ablated depth for photophysical ablation (solid) and for photothermal ablation (dashed).

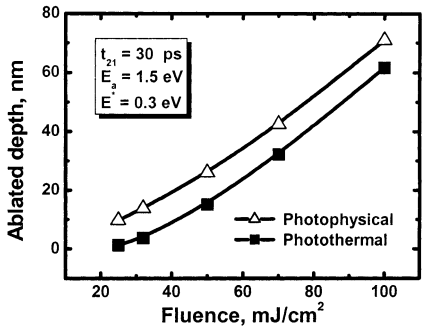


**Figure 21.** Ablated depth vs single pulse fluence for photophysical (upper curve) and photothermal ablation.

It is seen in Figure 19 that the time of the start of photophysical ablation is less than the thermal relaxation time.

Figure 21 demonstrates the ablated depth versus fluence for photophysical and photothermal models. It is seen that these curves go approximately parallel to each other. Thus, at high fluences the relative input of photophysical mechanism vanishes. The photophysical mechanism influences the ablated depth mainly at small fluences.

The photophysical addition to the ablated depth compared to one predicted by a pure photothermal model may be roughly estimated using the following considerations.

In considering a two-level model fluence $F \cong 15$ mJ/cm$^2$ is a saturating one. Above it the maximal surface temperature practically does not depend on fluence. Fluence determines only the width of absorbed laser energy distribution inside the material, scale length $\ell_s$. The maximal surface temperature roughly may be estimated to be $T_{max} \cong \hbar\omega n_0/c_p\rho + T_\infty$. Then the photophysically ablated length may be crudely approximated as

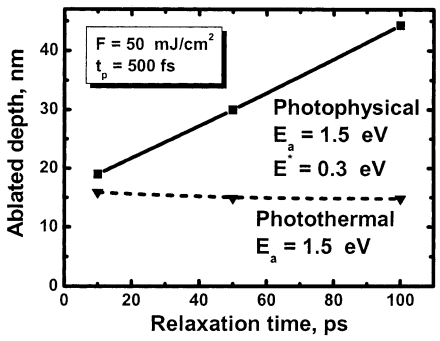


**Figure 22.** Ablated depth vs relaxation time. Fluence is 50 mJ/cm$^2$.

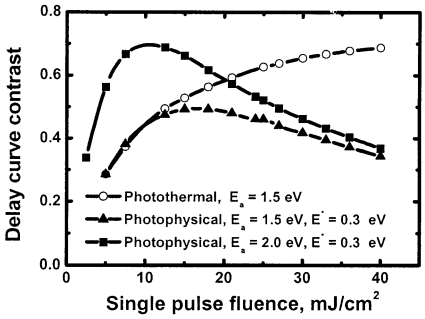


**Figure 23.** Different dependences of contrast (visuality) of delay curve (see text) on single pulse fluence for pure photothermal and photophysical ablation mechanisms.

$$h_{\mathrm{ph}} \approx V_0^* \exp(-E^*/k_{\mathrm{B}}T_{\max})t_{21} \qquad (172)$$

It is seen that this quantity does not depend on fluence. Of course, it is assumed that $h_{\mathrm{ph}} < \ell_{\mathrm{s}}$, where $\ell_{\mathrm{s}}$ can be roughly estimated as $\ell_{\mathrm{s}} \approx F/\hbar\omega n_0$.

After the end of relaxation the ablation proceeds as photothermal one. This qualitatively explains the course of curves in Figure 21.

The role of photophysical ablation increases with an increase in relaxation time. It can be seen, e.g., from the estimation (eq 172). In contrast, the photothermal model predicts a decrease in resulting ablated depth with an increase in relaxation time. It can be seen in Figure 22. This principal difference in predictions of photothermal and photophysical models unfortunately can hardly be observed experimentally since it is difficult to change relaxation time in a media without changing other parameters.

The delay curve for a photophysical model has been investigated in ref 47. One can characterize the delay curve by its contrast, i.e., by ratio $1 - h(t_{\mathrm{d}} = \infty)/h(t_{\mathrm{d}} = \infty)$. Here $h(t_{\mathrm{d}})$ stands for the ablated depth at delay time $t_{\mathrm{d}}$. "Infinity" here should be significantly smaller than the heat diffusion time and in our case it is approximately 200 ps. It has been shown in ref 47 that in the case of a pure surface photothermal model the contrast decreases with an increase in fluence. If ablation were pure photophysical, the contrast would increase with increasing fluence. It is seen in Figure 23. Here the increasing curve corresponds to the photophysical model with $E_{\mathrm{a}} = 2$ eV, $E^* = 0.3$ eV. The former value of activation energy causes the pure photothermal ablation to be suppressed and not to contribute to the resulting ablated depth. Thus, the ablation here is mainly photophysical. Figure 23 illustrates also the behavior of a delay curve for a pure photothermal model for fluencies higher than the saturating one. The photophysical model with $E_{\mathrm{a}} = 1.5$ eV provides intermediate results. The corresponding delay curve lies between the two discussed above. The reason is that the photophysical ablation here is followed by the photothermal ablation, which in the considered case of relatively small pure photothermal activation energy provides significant contribution into the resultant ablated depth.

In conclusion to this section, the dynamic of single USLP laser ablation that proceeds photophysically is essentially different from the dynamic of pure photothermal ablation. Nevertheless, the resulting ablated depths can be close if the activation energy of the pure photothermal process is not very high.

Electronic relaxation time significantly influences the effectiveness of photophysical ablation. An increase in relaxation time results in an essential increase of resultant etches depth in the case of photophysical ablation and slightly decreases the effectivity of pure photothermal ablation.

An experimental investigation of pair pulse laser ablation can give the information about the dominating mechanism. The contrast of a delay curve will increase with increasing single pulse fluence in the case of pure photophysical ablation and it demonstrates the opposite behavior in the case of a photothermal mechanism.

Nevertheless, the most important feature of photophysical ablation is that the delay time between the end of ultrashort laser pulse and the time of start of ablation is *less than thermal relaxation time* (compare to the results of the previous section C).

Most easily the photophysical ablation mechanism can be recognized in materials with long enough relaxation time and with the hindered pure photothermal ablation.

## V. Photochemical + Photothermal Models

Because of the controversial mechanism of laser ablation, attempts were made to construct models that take into consideration both photochemical and photothermal roots.

Thus, the "phenomenological" formula appears,[118] which suggests that the etch depth is the sum of the photochemical depth (1) and the photothermal depth, which obeys Arrhenius law.

This formula has not been derived from any physical consideration and in fact cannot be considered as modeling.

A more comprehensive consideration has been done in ref 119 where the bulk Stefan-like model of ablation was considered. Here the position of the ablation front was associated with the critical amount of broken bonds. The latter are created both by photothermal and by photochemical reaction of random direct chain scission.

It is more or less evident that at elevated temperatures the input of photochemical reactions will be negligible, thus this kind of models treats ablation as pure photochemical at small fluencies and pure photothermal at higher fluencies.

Some ideas about how to combine photothermal and photochemical reaction in the theory of laser ablation have been proposed in refs 120−122. We could formulate these approaches as follows.

The bulk reactions leading to ablation are photochemical, whereas the elimination of the products of these reactions from the surface is driven by temperature.

The second idea is that the quantum yield of photochemical bond breaking can depend on temperature. This is in agreement with the experimental findings of change in the yield of photochemical reaction of dye molecules incorporated in the PMMA matrix.[48,49] Of course, the mechanism of this change is not fully understood at the moment, but one of the possible driving forces could be elevated temperature.

As an example, we can formulate one of the possible models within the proposed approach and within the general approach developed in previous sections as follows.

Thus, we consider A → B chain-breaking model. Chain scission originates from both photothermal and photochemical processes. We assume a temperature-dependent quantum yield of photochemical reaction. For a moving interface, we accept the Frenkel-Wilson approach considered in section III.

All the designations are from sections III and IV.

$$\frac{\partial T}{\partial t} = V\frac{\partial T}{\partial z} + \frac{1}{\rho c_p(T)}\frac{\partial}{\partial z}\left[\kappa(T)\frac{\partial T}{\partial z}\right] + Q \qquad (173)$$

$$\frac{\partial n_B}{\partial t} = V\frac{\partial n_B}{\partial z} + \sigma_A\eta_A(T)(1 - n_B)\frac{I}{\hbar\omega} + (1 - n_B)k_0 \exp(-E_b/k_BT) \qquad (174)$$

$$Q = \frac{\alpha I}{c_p\rho} - \frac{\Delta H_{photo}N_0(1 - n_B)\sigma_A\eta_A(T)I}{c_p\rho\hbar\omega} - \frac{\Delta H_b N_0(1 - n_B)k_0 \exp(-E_b/k_BT)}{c_p\rho} \qquad (175)$$

$$\frac{\partial I}{\partial z} = -\alpha I \qquad (176)$$

$$\alpha = \sigma_A N_0(1 - n_B) + \sigma_B N_0 n_B \qquad (177)$$

$$V = V_{0m} \exp(-E_m/k_B n_s T_s) \qquad (178)$$

$$\kappa(T)\left.\frac{\partial T}{\partial z}\right|_{z=0} = \rho\Delta H_m V \qquad (179)$$

$$T|_{z\to\infty} = T_\infty,\ n_B|_{z\to\infty} = 0 \qquad (180)$$

The case $k_0 = 0$ corresponds to a pure photochemical model with a temperature-dependent quantum yield $\eta_A(T)$. This dependence can obey Arrhenius law.[123] This can be recognized as bulk photophysical reaction (see section IVD). Indeed, if an electronically excited state with the time of life $t_{21}$ can provide chain scission due to thermally activated process with activation energy $E^*$, then $\eta_A(T) \propto t_{21} \times \exp(-E^*/k_BT)$. Note that similar to our bulk photothermal model considered in section III the ablation velocity depends on both surface temperature and fraction of broken bonds on the surface. It is worth noting that if we neglect the heat then we return to the photochemical Frenkel-Wilson model considered in section II. Thus, all the formulas obtained in section II can be applied for the analysis of the model eqs 173−180.

Up to this point, we have been considering only random chain scission mechanism as a chemical pathway leading to ablation. Very intriguing is the unzipping mechanism of laser ablation. Unzipping is the process of depolymerization initiated by the creation of the radical at the end of the polymer chain. It is the main pathway of pyrolytic degradation of several addition polymers, i.e., polymers, which are obtained by polymerization, such as poly (tetrafluoroethylene), poly (methyl methacrylate), poly (α-methyl styrene).

Numerous experimental data on plume composition and pulse laser deposition of above addition polymers indicate that depolymerization is the main pathway in UV laser ablation of these polymers,[124−130] because of high content of monomer in the plume. Moreover, it was shown in ref 130 that even those addition polymers that pyrolyze by random scission producing little or no monomers provide high monomer yield being ablated by UV lasers.

It is now accepted by all the groups that study laser ablation of such polymers that initial chain scission and creation of radicals is provided photochemically, while radical depolymerization is driven by elevated temperature, i.e., photothermallty, because heating of the polymer is also provided by laser light. Thus, unzipping is one of the remarkable examples of combined photochemical and photothermal mechanisms.

## VI. The Role of Mechanical Stresses

Mechanical stresses caused by laser irradiation of polymers can strongly influence laser ablation of theses materials. Some authors consider mechanical stresses among the main driving forces of laser ablation of PMMA.[50,53,56,131,132] Specially designed photosensitive polymers are reported to be ablated through "explosive decomposition".[133] It means that here mechanical stresses play an important role.

The relevant stresses can be caused by different reasons. They can be thermoelastic stresses, emerging due to thermal expansion. They can also be provided by low-molecular products of both photochemical and photothermal bulk reactions. These species can result in quasistationary stress due to the increase of total molecular volume. The well-known example is depolymerization of PMMA. Polymerization of PMMA is accompanied by up to 20% of volume contraction.[134] It means that depolymerization should be accompanied by extension. On the other hand, the small, light, fragments, volatile species, consisting of simple molecules such as CO, CN, $CH_2$, etc., of number density $N_/$ may be treated as an ideal gas, which causes an average inner pressure

$$p = \zeta N_/ k_B T \qquad (181)$$

with $\zeta < 1$ (only a fraction of the total number of these species will contribute to $p$).

In the simplest case of uniaxial acoustic approximation when only stress tensor component $\sigma_{zz}$ is

relevant, the equation of thermoelasticity reads:

$$\frac{\partial^2\sigma_{zz}}{\partial t^2} = c_s^2\frac{\partial^2(\sigma_{zz} - p)}{\partial z^2} - \frac{E_Y}{3(1-2\mu)}\frac{\partial^2}{\partial t^2}[\alpha_V(T - T_0)] \quad (182)$$

Here $\alpha_V$ is the (volume) thermal expansion coefficient, $E_Y$ is Young's modulus, $\mu$ is the Poisson ratio, and $c_s$ is the sound velocity. Equation 182 should be solved together with the boundary conditions

$$\sigma_{zz}(t,z=0) = p(t,z=0),\ \sigma_{zz}(t,z=\infty) = 0 \quad (183)$$

Here $p$ is the quasistationary pressure, which for the case of volatile species obeys eq 181.

Stress can influence both the bulk photothermal bond breaking and material removal from the surface due to change in the corresponding activation energies. A simple estimation of this influence is provided by Zhurkov's formula (see e.g., ref 94), which reads that decrement of activation energy is linear with respect to stress. For example, in the case of a simple photothermal model we can write

$$E_a(\sigma) = E_a - \gamma\sigma \quad (184)$$

$$E_b(\sigma) = E_b - \gamma\sigma \quad (185)$$

In polymers, $\gamma$ can have values up to $10^{-21}$ cm$^3$ (for PMMA $\gamma = 1.7 \times 10^{-21}$ cm$^3$ [94]). Equation 185 is valid for tensile stress, i.e., when $\sigma > 0$. In the opposite case of compressive stress relation (eq 185) is not obvious, but a decrease in the activation energy of chain breaking is also possible due to local plastic deformations.[135]

Both eqs 184 and 185 are valid only if $E > \gamma\sigma$. In the opposite case, the chain breaking process will proceed independently of temperature with preexponential frequency. If $E_a < \gamma\sigma$, then the "sublimation" boundary condition is not valid. The particles will leave surface with sound and super sound velocities and gas-kinetics consideration should be applied.

As an example, let us consider the simple bulk photothermal model in quasistationary case, when transient stresses can be neglected. Typically, it is valid if pulse duration, $t_p$, is large enough: $t_p > 1/\alpha c_s$. Here $\alpha$ is absorption coefficient and $c_s$ is the sound velocity. We assume that the bulk photothermal reaction along with chain breaking process produces also $m$ volatile species and introduce $\beta_m = \zeta m$.

$$\frac{\partial T}{\partial t} = V\frac{\partial T}{\partial z} + \frac{1}{\rho c_p(T)}\frac{\partial}{\partial z}\left[\kappa(T)\frac{\partial T}{\partial z}\right] + Q \quad (186)$$

$$\frac{\partial n_B}{\partial t} = V\frac{\partial n_B}{\partial z} + (1 - n_B)k_0\exp(\gamma\beta n_B N_0)\exp(-E_b/k_B T) \quad (187)$$

$$Q = \frac{\alpha I}{c_p\rho} - \frac{\Delta H_b\left(1 - \frac{\gamma\beta n_B N_0 k_B T}{E_b}\right)N_0(1 - n_B)k_0\exp(-E_b/k_B T)}{c_p\rho} \quad (188)$$

$$V = V_{0m}\exp(\gamma\beta N_0)\exp(-E_m/k_B n_s T_s) \quad (189)$$

$$I(0,t) = I_0(t)\exp[-\alpha_p h(t)] \quad (190)$$

$$\frac{\partial I}{\partial z} = -\alpha I \quad (191)$$

$$\kappa(T)\frac{\partial T}{\partial z}\Big|_{z=0} = \rho\Delta H_m\left(1 - \gamma\frac{\beta n_s N_0 k_B T_s}{E_m}\right)V \quad (192)$$

$$T|_{z\to\infty} = T_\infty,\ n_B|_{z\to\infty} = 0 \quad (193)$$

For short pulses when $t_p < 1/\alpha c_s$ (for ultrashort laser pulses considered in section IV, we should take here thermal relaxation time rather than pulse duration) nonstationary effects, caused by transient stresses are relevant. These stresses can result in spallation, i.e., in the removal of a part of material due to propagation of rarefaction wave, as it was demonstrated in ref 56, where the film of PMMA as a whole was removed from substrate by such a way.

Transient stresses also can provide bulk chain degradation. Some possible nonstationary effects when photophysical phenomena are accompanied by transient stresses are considered in refs 57 and 58. Some possible effects of recoil pressure on generation of broken bonds were also discussed there.

When examining the bulk photothermal model in the form studied in sections III and IV and applying it to specific materials, estimations should be performed whether the effect of stresses is significant or not. For example, it was shown in ref 136 that for polyimide near ablation threshold both nonstationary thermoelastic stresses and quasistationary stresses resulting from pressure provided by heated volatile species, can be neglected from the point of chain scission if $\gamma < 3 \times 10^{-21}$ cm$^3$ and $\beta_m < 0.1$.

With PMMA there is, as pointed out by several authors,[131,137] a contradiction between data on photochemical modification with fluencies well below ablation threshold and near ablation threshold. With small laser fluencies or when PMMA is irradiated by UV lamps there are a lot of evidences published that UV photon being absorbed by ester group (this is a side group on PMMA main chain) results in cleavage of this group with small (~0.01) quantum yield of the main chain scission.[14,77,138,139] The data of authors of refs 131 and 137 on modification of PMMA by laser pulses with fluences close to the ablation threshold allow these authors to point out that the chain scission process initializing depolymerization is much more effective. One possible explanation of this phenomenon is that inner mechanical stresses originated from both the extraction of unzipped monomers and the creation of volatile species during cleavage of side ester group together with heating provided by laser irradiation can influence, increase, the quantum yield of photochemical chain breaking. Moreover, the activation energy of the initial pure thermal chain breaking process can decrease due to arising mechanical stresses also facilitating creation of the end radicals initiating the unzipping process.

Up to now, we considered some averaged macrostresses. But at the moment of emerging of monomer during unzipping or at the moment of cleavage of a

particular side group and escape of volatile species, the occurring micro-stresses can be large enough to provide some chemical changing of adjacent molecules. Molecular dynamic simulations of some of these processes are performed in papers.[50,59]

There is another interesting problem connected with the influence of stresses, namely, ablation in the presence of outer stresses.[140−143] Here ablation is unstable resulting in surface pattering and cracks formation.

## VII. Conclusions

Laser ablation of polymers is closely related to chemical degradation of polymers caused by laser irradiation. The existing knowledge on both photochemical and thermal degradation and stabilization of polymers could be taken into account as a chemical background when modeling this phenomenon. However, UV laser irradiation provides conditions within the materials which significantly differ from those of usual experiments either pyrolytic or photochemical.

This is connected with relatively high power density of irradiation by short, nanosecond, picosecond, and even femtosecond, pulses. Using these short laser pulses, one can create a very high temperature within a very small volume of polymer. These temperatures simply cannot be reached with conventional techniques, because polymers do not exist at such temperatures for a relatively long time. High laser intensity also allows creation of numerous electronically excited species, high mechanical pressure, and some other effects, which can result in change of chemical pathways.

Physics of laser−matter interactions, on the other hand, has much experience with laser ablation and modification of nonpolymeric materials. Our approach is to incorporate, as far as it is possible, the specific features of polymers within the framework of models that have been developed for other materials.

Among the features that should be taken into account we can mention, for example, the electronic structure of polymers. In the majority of polymers, UV photons are absorbed by chromophores in which several first levels of electronic excitation belong to the bound states.

Another specific feature is a hierarchy of bonds between neighboring molecular groups, namely, strong, covalent bonds within a polymer chain and relatively weak molecular bonds between neighbor molecular groups that belong to different chains.

One more important point is that chemical reactions in polymer materials are often accompanied by the creation of low-molecular, volatile, species. This is of importance if we take into account that amorphous polymer solids generally contain a significant amount of free volume. These features have a considerable influence upon laser ablation of polymers.

In the present paper, we have developed a set of relatively simple models, which permit to understand basic features of laser ablation and even describe some experiments with sufficient accuracy. Despite the complexity of the discussed problem, this "step by step" approach seems to be constructive.

The modeling of laser ablation of polymers is yet far from its completion. Nevertheless, some conclusions can be drawn. First, the etch kinetic curve, i.e., the dependence of etch depth versus laser fluence, being the most popular objective of experimental works, is not sensitive to the mechanism of ablation. Fitting of these experimental data by one or another theoretical model is not an argument that this particular model really works. It is only a necessary but not sufficient condition. More informative are data on dynamics of laser ablation and on surface temperature.

No doubt that more complex numerical experiments also can be performed to establish agreement between the theory and experiment.

## VIII. Acknowledgment

The authors express their appreciation to Prof. S. Anisimov, Prof. D. Bäuerle, Dr. N. Arnold, Dr. M. C. Castex, Dr. A. Malyshev, Dr. S. Georgiou, and Dr. T. Lippert for many discussions. Part of this work was done under support of the Russian Foundation for Basic Research (Grants No. 01-02-16136 and No. 02-02-17745).

## IX. References

(1) Srinivasan, R.; Mayne-Banton, V. *Appl. Phys. Lett.* **1982**, *41*, 576.
(2) Kawamura, Y.; Toyoda, K.; Namba, S. *Appl. Phys. Lett.* **1982**, *40*, 374.
(3) Srinivasan, R.; Braren, B. *Chem. Rev.* **1989**, *89*, 1303.
(4) Miller, J. C.; Haglung, R., Jr., Eds. *Laser Ablation − Mechanisms and Applications*; Springer-Verlag: Berlin, 1991.
(5) Fogarassy, E.; Lazare, S. *Laser Ablation of Electronic Materials − Basic Mechanisms and Applications*; Elsevier: Amsterdam, 1992.
(6) Lazare, S.; Granier, V. *Laser Chem.* **1989**, *10*, 25.
(7) Bäuerle, D. *Laser Processing and Chemistry*, 3rd ed; Springer-Verlag: Berlin, 2000.
(8) Andrew, J. E.; Dyer, P. E.; Forster, D.; Key, P. H. *Appl. Phys. Lett.* **1983**, *43*, 717.
(9) Deutsch, T. F.; Geis, M. W. *J. Appl. Phys.* **1983**, *54*, 7201.
(10) Jellinek, H. H. G.; Srinivasan, R. *J. Phys. Chem.* **1984**, *88*, 3048.
(11) Dijkkamp, D.; Gozdz, A. S.; Venkatesan, T.; Wu, X. D. *Phys. Rev. Lett.* **1987**, *58*, 2142.
(12) Oldershaw, G. A. *Chem. Phys. Lett.* **1991**, *186*, 23.
(13) Küper, S.; Brannon, J.; Brannon, K. *Appl. Phys. A* **1993**, *56*, 43.
(14) Küper, S.; Stuke, M. *Appl. Phys. A* **1989**, *49*, 211.
(15) Pettit, G. H.; Sauerbrey, R. *Appl. Phys. Lett.* **1991**, *58*, 793.
(16) Pettit, G. H.; Sauerbrey, R. *Appl. Phys. A* **1993**, *56*, 51.
(17) Pettit, G. H.; Ediger, M. N.; Hahn, D. W.; Brinson, B. E.; Sauerbrey, R. *Appl. Phys. A* **1994**, *58*, 573.
(18) Lippert, T.; Bennett, L. S.; Nakamura, T.; Niino, H.; Ouchi, A.; Yabe, A. *Appl. Phys. A* **1996**, *63*, 257.
(19) Mansour, N.; Ghaleb, K. J. *Appl. Phys. A* **2002**, *74*, 63.
(20) D'Couto, G. C.; Babu, S. V. *J. Appl. Phys.* **1994**, *76*, 3052.
(21) Cain, S. R.; Burns, F. C.; Otis, C. E. *J. Appl. Phys.* **1992**, *71*, 4107.
(22) Cain, S. R.; Burns, F. C.; Otis, C. E.; Braren, B. *J. Appl. Phys.* **1993**, *72*, 5172.
(23) Cain, S. R. *J. Phys. Chem.* **1993**, *97*, 7572.
(24) Masubuchi, T.; Tada, T.; Nomura, E.; Hatanaka, K.; Fukumura, H.; Masuhara, H. *J. Phys. Chem. A* **2002**, *106*, 2180.
(25) Anisimov, S. I.; Imas, Ya. A.; Romanov, G. S.; Khodyko, Yu. V. *Action of High-Power Radiation on Metal*; National Technical Information Service, Springfield, Virginia, 1971.
(26) Keyes, T.; Clarke, R. H.; Isner, J. M. *J. Phys. Chem.* **1985**, *89*, 4194.
(27) Sutcliffe, E.; Srinivasan, R. *J. Appl. Phys.* **1986**, *60*, 3315.
(28) Mahan, G. D.; Cole, H. S.; Liu, Y. S.; Philipp, H. R. *Appl. Phys. Lett.* **1988**, *53*, 2377.
(29) Lazare, S.; Granier, V. *Appl. Phys. Lett.* **1988**, *54*, 862.
(30) Schildbach, K. *Proc. SPIE* **1990**, *1279*, 60.
(31) Kleinschmidt, J.; Walther, J.-U. *Phys. Stat. Sol. (a)* **1992**, *131*, 167.

(32) Furzikov, N. P. *Appl. Phys. Lett.* **1990**, *56*, 1638.
(33) Bäuerle, D.; Luk'yanchuk, B.; Schwab, P.; Wang, X. Z.; Arenholz, E. In *Laser Ablation of Electronic Materials − Basic Mechanisms and Applications*; Elsevier: Amsterdam, 1992; p 39.
(34) Tokarev, V. N.; Lunney, J. G.; Marine, W.; Sentis, M. *J. Appl. Phys.* **1995**, *78*, 1241.
(35) Luk'yanchuk, B.; Bityurin, N.; Himmelbauer, M.; Arnold, N. *Nucl. Instr. Methods B* **1997**, *122*, 347.
(36) Arnold, N.; Luk'yanchuk, B.; Bityurin, N. *Appl. Surf. Sci.* **1998**, *127*, 184.
(37) Bityurin, N. *Appl. Surf. Sci.* **1999**, *138−139*, 354.
(38) Castex, M. C.; Bityurin, N.; Olivero, C.; Muraviov, S.; Bronnikova, N.; Riedel, D. *Appl. Surf. Sci.* **2000**, *168*, 175.
(39) Castex, M. C.; Bityurin, N. *Appl. Surf. Sci.* **2002**, *197−198*, 805.
(40) Bityurin, N.; Castex, M. C. *J. Appl. Phys.* **2003**, in press.
(41) Bityurin, N.; Arnold, N.; Luk'yanchuk, B.; Bäuerle, D. *Appl. Surf. Sci.* **1998**, *127*, 164.
(42) Arnold, N.; Bityurin, N. *Appl. Phys. A* **1999**, *68*, 615.
(43) Bityurin, N. *Proc. SPIE.* **2001**, *4423*, 197.
(44) Bityurin, N.; Malyshev, A. *J. Appl. Phys.* **2002**, *92*, 605.
(45) Luk'yanchuk, B.; Bityurin, N.; Anisimov, S.; Bäuerle, D. *Appl. Phys. A* **1993**, *57*, 367.
(46) Luk'yanchuk, B.; Bityurin, N.; Anisimov, S.; Arnold, N.; Bäuerle, D. *Appl. Phys. A* **1996**, *62*, 397.
(47) Luk'yanchuk, B.; Bityurin, N.; Malyshev, A.; Anisimov, S.; Arnold, N.; Bäuerle, D. *Proc. SPIE* **1998**, *3343*, 58.
(48) Lassithiotaki, M.; Athanassiou, A.; Anglos, D.; Georgiou, S.; Fotakis, C. *Appl. Phys. A* **1999**, *69*, 363.
(49) Athanassiou, A.; Lassithiotaki, M.; Anglos, D.; Georgiou, S.; Fotakis, C. *Appl. Surf. Sci.* **2000**, *154−155*, 89.
(50) Garrison, B. J.; Srinivasan, R. *Appl. Phys. Lett.* **1984**, *44*, 849.
(51) Garrison, B. J.; Srinivasan, R. *J. Appl. Phys.* **1985**, *57*, 2909.
(52) Gorodetsky, G.; Kazyaka, T. G.; Melcher, R. L.; Srinivasan, R. *Appl. Phys. Lett.* **1985**, *46*, 828.
(53) Kitai, M. S.; Popkov, V. L.; Semchishen, V. A. *Makromol. Chem. Macromol. Symp.* **1990**, *37*, 257.
(54) Zweig, A. D.; Venugopalan, V.; Deutsch, T. F. *J. Appl. Phys.* **1993**, *74*, 4181.
(55) Hare, D. E.; Dlott, D. D. *Appl. Phys. Lett.* **1994**, *64*, 715.
(56) Hare, D. E.; Franken, J.; Dlott, D. D. *J. Appl. Phys.* **1995**, *77*, 5950.
(57) Bityurin, N.; Malyshev, A.; Luk'yanchuk, B.; Anisimov, S.; Baeuerle, D. *Proc. SPIE* **1996**, *2802*, 103.
(58) Luk'yanchuk, B.; Bityurin, N.; Anisimov, S.; Malyshev, A.; Arnold, N.; Baeuerle, D. *Appl. Surf. Sci.* **1996**, *106*, 120.
(59) Zhigiley, L. V.; Kodali, P. B.; Garrison, B. J. *J. Phys. Chem. B* **1998**, *102*, 2845.
(60) Albagli, D.; Dark, M.; Perelman, L. T.; von Rosenberg, C.; Itzkan, I.; Feld, M. S. *Opt. Lett.* **1994**, *19*, 1684.
(61) Anisimov, S. I.; Luk'yanchuk, B. S. *Physics-Uspekhi* **2002**, *45*, 293.
(62) Braren, B.; Casey, K. G.; Kelly, R. *Nucl. Instr. Methods B* **1991**, *58*, 463.
(63) Kelly, R.; Braren, B. *Appl. Phys. B* **1991**, *53*, 160.
(64) Afanasiev, Y. V.; Isakov, V. A.; Zavestovskaya, I. N.; Chichkov, B. N.; von Alvensleben, F.; Welling, H. *Appl. Phys. A* **1997**, *64*, 561.
(65) Kitai, M. S.; Semchishen, V. A. *Quantum Electron.* **1996**, *26*, 517.
(66) Hodapp, T. W.; Fleming, P. R. *J. Appl. Phys.* **1998**, *84*, 577.
(67) Luk'yanchuk, B.; Bityurin, N.; Anisimov, S.; Baeuerle, D. *Appl. Phys. A* **1993**, *57*, 449.
(68) Bolle, M.; Lazare, S.; Leblank, M.; Wilmes, A. *Appl. Phys. Lett.* **1992**, *60*, 674.
(69) Lazare, S.; Bolle, M.; Cros, A.; Bellard, L. *Nucl. Instr. Methods B* **1995**, *105*, 159.
(70) Hiraoka, H.; Gendova, M. *Appl. Phys. Lett.* **1994**, *64*, 563.
(71) Dyer, P. E.; Farley, R. J.; Giedl, R.; Ragdale, C.; Reid, D. *Appl. Phys. Lett.* **1994**, *64*, 3389.
(72) Dyer, P. E.; Karnakis, D. M.; Oldershaw, G. A. *Appl. Surf. Sci.* **1995**, *86*, 1.
(73) Mauser, H. *Z. Naturforsch.* **1967**, *22B*, 569.
(74) Mauser, H. *Z. Naturforsch.* **1979**, *34C*, 1264.
(75) Bityurin, N. M. Ph.D. Thesis, Inst. Appl. Phys., USSR Ac. Sci., Gorkii, USSR, 1988.
(76) Bityurin, N. M.; Genkin, V. N.; Sokolov, V. V. *Sov. J. Polymer Sci. (Vysokomol. Soedin.)* **1982**, *24A*, 748.
(77) Bityurin, N.; Muraviov, S.; Alexandrov, A.; Malyshev, A. *Appl. Surf. Sci.* **1997**, *110*, 270.
(78) Bityurin, N.; Muraviov, S.; Alexandrov, A.; Bronnikova, N.; Malyshev, A. *Proc. SPIE* **1997**, *3093*, 108.
(79) Dyer, P. E.; Oldershaw, G. A.; Schudel, D. *J. of Phys. D − Appl. Phys.* **1993**, *26*, 323.
(80) Lapczyna, M.; Stuke, M. *Appl. Phys. A* **1998**, *66*, 473.
(81) Museur, L.; Zheng, W. Q.; Kanaev, A. V.; Castex, M. C. *IEEE J. Sel. Top. Quantum Electron.* **1995**, *1*, 900.
(82) Riedel, D.; Castex, M. C. *Appl. Phys. A* **1999**, *69*, 375.
(83) Tinone, M. C. K.; Tanaka, K.; Ueno, N. *J. Vac. Sci. Technol.* **1995**, *13*, 1885.
(84) Valiev, K. A.; Velikov, L. V.; Dorofeev, Yu. I.; Skurat, V. E. *Chem. High Energy* **1988**, *22*, 352.
(85) White, J. C.; Craighead, H. G.; Howard, R. E.; Jackel, L. D.; Beringer, R. E.; Epworth, R. W.; Henderson, D.; Sweeney, J. E. *Appl. Phys. Lett.* **1984**, *44*, 22.
(86) Kudo, K.; Iwabuchi, T.; Muton, K.; Miyata, T.; Sano, R.; Tanaka, K. *Jpn. J. Appl. Phys.* **1990**, *29*, 2572.
(87) Zienkiewicz, O. C. *The Finite Element Method*; McGraw-Hill: New York, 1977.
(88) Zwillinger, D. *Handbook of Differential Equations*; Academic Press: Boston, 1989.
(89) Karlov, N. V.; Kirichenko, N. A.; Luk'yanchuk, B. S. *Laser Thermochemistry*; Cambridge International Science Press: 2000.
(90) Arnold, N.; Luk'yanchuk, B.; Bityurin, N.; Bäuerle, D. *Proc. SPIE* **1998**, *3343*, 484.
(91) Wolfram, S. *Mathematica*, 4th ed; Wolfram Media/Cambridge University Press, 1999.
(92) Luk'yanchuk, B.; Bityurin, N.; Anisimov, S.; Bäuerle, D. In *Excimer Lasers*; Laude, L. D., Ed.; Kluwer Academic Publishers: Dordrecht, 1994; p 59.
(93) Brunco, D. P.; Thompson, M. Q.; Otis, C. E.; Goodwin, P. M. *J. Appl. Phys.* **1992**, *72*, 434.
(94) Bartenev, G. M. *Stability and Mechanisms of Polymer Destruction*; Khimia, Moscow, 1984 (in Russian).
(95) Guillet, J. *Polymer Photophysics and Photochemistry*; Cambridge University Press: Cambridge, 1985.
(96) Srinivasan, R.; Hall, R. R.; Loehle, W. D.; Wilson, W. D.; Allbee, D. C. *J. Appl. Phys.* **1995**, *78*, 4881.
(97) Ball, Z.; Feurer, T.; Callahan, D. L. Sauerbrey, R. *Appl. Phys. A* **1996**, *62*, 203.
(98) Lazare, S.; Guan, W.; Drilhole, D. *Appl. Surf. Sci.* **1996**, *96−98*, 605.
(99) Taylor, R. S.; Singleton, D. L.; Paraskevopoulos, G. *Appl. Phys. Lett.* **1987**, *50*, 1779.
(100) Samarskii, A. A.; Vabishchevich, P. N. *Computational Heat Transfer*; John Wiley: New York, 1995.
(101) Himmelbauer, M.; Bityurin, N.; Luk'yanchuk, B.; Arnold, N.; Bäuerle, D. *Proc. SPIE* **1997**, *3093*, 220.
(102) Ortelli, E. E.; Geiger, F.; Lippert, T.; Wei, J.; Wokaun, A. *Macromolecules* **2000**, *33*, 5090.
(103) Babu, S. V.; D'Couto, G. C.; Egitto, F. D. *J. Appl. Phys.* **1992**, *72*, 692.
(104) Himmelbauer, M.; Arenholz, E.; Bäuerle, D. *Appl. Phys. A* **1996**, *63*, 87.
(105) Paraskevopoulos, G.; Singleton, D. L.; Irwin, R. S.; Taylor, R. S. *J. Appl. Phys.* **1991**, *70*, 1938.
(106) Himmelbauer, M.; Arenholz, E.; Bäuerle, D.; Schichler, K. *Appl. Phys. A* **1996**, *63*, 337.
(107) Preuss, S.; Spaeth, M.; Zhang, Y.; Stuke, M. *Appl. Phys. Lett.* **1993**, *62*, 3049.
(108) Kautek, W.; Krueger, J.; Lenzner, M.; Sartania, S.; Spielman, Ch.; Krausz, F. *Appl. Phys. Lett.* **1996**, *69*, 3146.
(109) Stuart, B. C.; Feit, M. D.; Rubenchik, A. M.; Shore, B. W.; Perry, M. D. *Phys. Rev. Lett.* **1995**, *74*, 2248.
(110) Oraevsky, A. A.; DaSilva, L. B.; Feit, M. D.; Glinsky, M. E.; Mammini, B. M.; Paquette, K. L.; Perry, M. D.; Rubenchik, A. M.; Small, W.; Stuart, B. C. *Proc. SPIE* **1995**, *2391*, 423.
(111) Stuart, B. C.; Feit, M. D.; Herman, S.; Rubenchik, A. M.; Shore, B. W.; Perry, M. D. *JOSA B* **1996**, *13*, 459.
(112) Bityurin, N.; Malyshev, A. *Appl. Surf. Sci.* **1998**, *127−129*, 199.
(113) Malyshev, A. Yu.; Bityurin, N. M. *Quantum Electron.* **1999**, *29*, 134.
(114) Frisoli, J. K.; Hefetz, Y.; Deutsch, T. F. *Appl. Phys. B* **1991**, *52*, 168.
(115) Rosenfeld, A.; Ashkenasi, D.; Varel, H.; Wähmer, M.; Cambell, E. E. B. *Appl. Surf. Sci.* **1998**, *127−129*, 76.
(116) Stoian, R.; Ashkenasi, D.; Rosenfeld, A.; Campbell, E. E. B. *Phys. Rev. B* **2000**, *62*, 13167.
(117) Stoian, R.; Boyle, M.; Thoss, A.; Rosenfeld, A.; Ashkenasi, D.; Korn, G.; Hertel, I. V.; Campbell, E. E. B. In *Technical Digest CLEO'2001*, Baltimore, MD, Baltimore Convention Center, May 6−11, 2001, p 577.
(118) Srinivasan, V.; Smrtic, M. A.; Babu, S. V. *J. Appl. Phys.* **1986**, *59*, 3861.
(119) Schmidt, H.; Ihlemann, J.; Wolff-Rottke, B.; Luther, K.; Troe, J. *J. Appl. Phys.* **1998**, *83*, 5458.
(120) Dyer, P. E.; Sidhu, J. *J. Appl. Phys.* **1985**, *57*, 1420.
(121) Kalontarov, L. I. *Phylos. Magn. Lett.* **1991**, *63*, 289.
(122) Kalontarov, L. I.; Marupov, R. *Chem. Phys. Lett.* **1992**, *196*, 15.
(123) Shlapintokh, V. Ya. *Photochemical Conversion and Stabilization of Polymers*; Hanser Publishers: New York, 1984.
(124) Blanchet, G. B.; Fincher, C. R., Jr. *Appl. Phys. Lett.* **1994**, *65*, 1311.
(125) Blanchet, G. B.; Shah, I. *Appl. Phys. Lett.* **1993**, *62*, 1026.
(126) Dickinson, J. T.; Jaw-Jung, Shin; Jiang, W.; Norton, M. G. *J. Appl. Phys.* **1993**, *74*, 4729.
(127) Dickinson, J. T.; Jaw-Jung, Shin; Jiang, W.; Norton, M. G. *Nucl. Instr. Methods B* **1994**, *91*, 672.

(128) Tsunekava, M.; Nishio, S.; Sato, H. *Jpn. J. Appl. Phys.* **1995**, *34*, 218.
(129) Blanchet, G. B.; Fincher, C. R., Jr. *Appl. Phys. Lett.* **1996**, *68*, 929.
(130) Blanchet, G. B. *J. Appl. Phys.* **1996**, *80*, 4082.
(131) Srinivasan, R.; Braren, B.; Casey, K. G. *J. Appl. Phys.* **1990**, *68*, 1842.
(132) Hare, D. E.; Dlott, D. D. *Appl. Phys. Lett.* **1994**, *64*, 715.
(133) Bennet, L. S.; Lippert, T.; Furutani, H.; Fukumura, H.; Masuhara, H. *Appl. Phys. A* **1996**, *63*, 327.
(134) Odian, G. *Principle of Polymerization*, 2nd ed; Wiley: New York, 1970; p. 258.
(135) Zeldovich, Ya. B.; Raizer, Yu. P. *Physics of Shock Waves and High-Temperature Hydrodynamic Phenomena*; New York, Academic Press: 1966−1967, 2 vols.
(136) Malyshev, A. *Ph.D. Thesis*, Inst. Appl. Phys. Russian Ac. Sci., N. Novgorod, 2002.
(137) Blanchet, G. B.; Cotts, P.; Fincher, C. R., Jr. *J. Appl. Phys.* **2000**, *68*, 2975.
(138) Mikheev, Yu. A.; Popravko, T. S.; Toptygin, D. Ya. *Doklady AN SSSR* **1973**, *210*, 148.
(139) Gupta, A.; Liang, R.; Tsay, F. D.; Moacanin, J. *Macromolecules* **1980**, *13*, 1696.
(140) Tonyali, K.; Jensen, L. C.; Dickinson, J. T. *J. Vac. Sci. Technol. A* **1988**, *6*, 941.
(141) Bahners, T.; Schollmeyer, E. *J. Appl. Phys.* **1989**, *66*, 1884.
(142) Arenholz, E.; Wagner, M.; Heitz, J.; Bäuerle, D. *Appl. Phys. A* **1992**, *55*, 119.
(143) Bityurin, N.; Arenholz, E.; Arnold, N.; Bäuerle, D., to be published.
(144) Aksenov, V. P.; Mikhailova, G. N.; Boneberg, J.; Leiderer, P.; Muenzer, H. J. *Proc. SPIE* **2001**, *4423*, 70.

CR010426B